https://doi.org/10.5194/egusphere-2025-5197
Preprint. Discussion started: 30 January 2026

Evaluation of the LandscapeDNDC model for drained peatland forest managements, LDNDC v1.35.2 (revision 11434)

Ahmed Hasan Shahriyer[1], David Kraus[2], Tiina Markkanen[1], Mika Korkiakoski[1], Helena Rautakoski[1], Suvi Orttenvuori[1], Yao Gao[3], Henri Kajasilta[1], Rüdiger Grote[2], Annalea Lohila[1,4], and Tuula Aalto[1]

[1]Climate System Research, Finnish Meteorological Institute, Helsinki, Finland
[2]Institute of Meteorology and Climate Research Atmospheric Environmental Research (IMKIFU), Karlsruhe Institute of Technology, Garmisch-Partenkirchen, Germany
[3]Department of Civil Engineering, University of Hongkong, Hongkong, China
[4]Institute for Atmospheric and Earth System Research/Physics (INAR), Faculty of Science, P.O. Box 68, 00014 University of Helsinki, Helsinki, Finland

Correspondence: Ahmed Hasan Shahriyer (ahmed.hasan.shahriyer@fmi.fi)

Abstract. Rotational forestry (RF) is the prevailing management practice on drained peatlands in Finland, while continuous cover forestry (CCF) is increasingly studied for its potential climate benefits. We applied the process-based LandscapeDNDC model, for the first time, to simulate experimental peatland forest stands under three different managements: RF, CCF and non-managed control. Mixed-species stands of pine, spruce, and birch were initialized, with management, partial harvest of pine in CCF and clear-cut harvest of all species in RF, leading to species shifts toward spruce–birch dominance in CCF and birch seedlings in RF. The primary objective of this study was to evaluate the performance of LandscapeDNDC model in forested drained peatlands. To this aim, we quantified the differences in gas exchange and water balance originating from differences in species composition and management methods. We also implemented modification to dynamic water table (WT) calculations and improved humus pool partitioning based on soil carbon-to-nitrogen ratios. Model evaluation against field data showed strong agreement for daily net ecosystem exchange (correlation 0.84–0.88; Nash–Sutcliffe efficiency 0.66–0.75). Modeled leaf area index (LAI) closely matched site estimates before management and Sentinel-2 satellite estimated LAI afterwards. Soil moisture and WT dynamics were realistically reproduced. Methane flux patterns were accurately captured in the control and CCF stands. Moreover, the methane flux was found to be sensitive to the WT after clear-cut in the RF stand. Modeled annual carbon balances were consistent with measurements and indicated that CCF became a carbon sink more rapidly than RF. These results demonstrate that LandscapeDNDC can reliably simulate the biogeochemical and hydrological consequences of alternative peatland forest management scenarios. The model therefore provides a valuable tool for developing climate-smart management strategies on drained peat soils.

1 Introduction

Peatlands cover 3% of the land area on Earth (Clarke and Rieley, 2019). The amount of carbon stored in northern peatlands is estimated to be around 1016–1105 Gt (Nichols and Peteet, 2019). Peatlands are often drained for use in forestry, agriculture, and peat extraction (Clarke and Rieley, 2019). In Finland, peatland drainage began in the 1920s and increased significantly

https://doi.org/10.5194/egusphere-2025-5197
Preprint. Discussion started: 30 January 2026

in the 1960s. The drainage of peatlands expands the land area available for forestry, facilitating tree growth in regions that were previously unsuitable for productive forest development. However, draining peatlands leads to increased aeration and degradation of the peat, which increases carbon dioxide (CO_2) emissions from the soil due to increased peat decomposition (Findlay, 2021). Forests on drained peatlands make up 25% (5.7 Mha) of the total forested land area in Finland (Turunen and Valpola, 2020).

Soils on drained, nutrient-rich sites tend to be sources of CO_2. Emissions from peat soil are often offset by carbon fixation by the forest, at least on nutrient-poor sites (Ojanen et al., 2013). However, it may take decades for the forest to reach net CO_2 sink after drainage, if it is reached at all. Drained fen-type peatlands contain nutrient-rich peat soils compared to nutrient-poor bog-type peatlands. The carbon-to-nitrogen ratio (C:N) is an often-used indicator for the nutrient status and it is typically lower in drained fens indicating nutrient-richness. The decomposition of peat releases nutrients available to plants and this nutrient input decreases from rich to poorer sites.

Carbon storage of the forest ecosystem is also subject to management practices. When the forest is harvested, most of the carbon stored in wood is rapidly lost to the atmosphere if the harvested wood is used for short-lifetime products such as pulp or energy production (Makrickas et al., 2023). Therefore, a peatland forest, whose soil is a net CO_2 source, has a climate warming impact over the entire forest rotation period, even though it may be a net CO_2 sink at a moment in time.

The most common forest management method implemented in Nordic countries has been Rotational Forestry (RF). In RF, forests are clear-cut when a specific stand volume has been reached and new stands are usually established by planting seedlings on the harvested land (Nieminen et al., 2018). Before planting new seedlings, the harvested land is sometimes fertilized and mounded, and often the mounding material comes from ditch maintenance (Hytönen et al., 2020). Harvest residues (litter, small branches, tree roots and stumps from the previous forest) are often left on the site or removed. Recently, more importance has been given to the investigation and implementation of alternative forestry management methods that would decrease carbon losses from the soil while maintaining profitable timber production. Continuous Cover Forestry (CCF) has been suggested as a management practice that could be applied to reach this goal (Nieminen et al., 2018). In CCF, the forest is never clear-cut as in RF, but rather selectively harvested depending on the forest and soil characteristics, resulting in an unevenly aged forest structure.

In drained peatlands, vegetation growth significantly influences the water table (WT) through evapotranspiration. Increased biomass, particularly from deep-rooted trees, promotes water loss, leading to a decrease in WT (Laiho, 2006). In CCF, the WT remains higher than in the full-grown forest (Sarkkola et al., 2010), reducing peat degradation and minimizing the carbon loss from the soil. Ditch management costs, which are often necessary after clear-cut, can also be avoided as the remaining trees in the CCF continue to transpire water, keeping the WT low enough not to hinder tree growth (Nieminen et al., 2018). An increase in WT could lead to higher anaerobic conditions in the soil layer that promote methanogenesis and eventually even turn drained peatlands into a net CH_4 source (Lohila et al., 2011). Temporal and spatial variations of CH_4 can be attributed to the dynamics of soil temperature, WT and vegetation communities (Minkkinen and Laine, 2006).

Measurements of the net ecosystem carbon exchange in Lettosuo showed that mature forest on drained peatland, which was a small sink of CO_2 before harvest, can become a bigger CO_2 source after harvest if the site is under RF management compared

https://doi.org/10.5194/egusphere-2025-5197
Preprint. Discussion started: 30 January 2026

to CCF (Korkiakoski et al., 2023). Same site was a sink for CH_4 due to low WT before harvest (Korkiakoski et al., 2017) and a source of CH_4 after harvest (clear-cutting, (Korkiakoski et al., 2019)).

Apart from being a major habitat, peatland systems have challenged terrestrial ecosystem models (Mozafari et al., 2023; Silva et al., 2024), for example because of their dynamic water table regulating carbon processes (e.g., Mezbahuddin et al., 2017), or specific ground vegetation (e.g., Shi et al., 2021). Only in recent years, specific processes for peatlands have been given more consideration (e.g., Liu et al., 2022; Li et al., 2024). The process-based ecosystem model LandscapeDNDC has been used to simulate carbon and water balances in various forest systems, including monoculture (Werner et al., 2012; Dirnböck et al., 2016), structured forests with ground vegetation (Dirnböck et al., 2020; Cade et al., 2021) and managed forests (Grote et al., 2011). The simulations mentioned above considered sites with mineral soils, whereas applications on peat soils are still lacking.

The primary objective of this study is to evaluate the performance of LandscapeDNDC model in forested drained peatlands. To address this objective, we refined and employed a process-based model, applied here for the first time to a nutrient-rich drained peatland in Finland. Refinements to the dynamic WT and high carbon content are investigated using carbon and water flux measurements. We perform a sensitivity analysis to determine the most sensitive parameters for decomposition in carbon rich soil. We assess how variations in tree species composition and management methods influence gas exchange and water balance. The model improvements should allow for a realistic representation of the forest CO_2 and CH_4 budgets, soil hydrology, and soil carbon balances within the drained peatland forest systems. Ultimately, the study aims not only to test the model's applicability and accuracy for Lettosuo study site but also to provide a foundation for assessing future peatland management scenarios. This approach supports the broader goal of identifying climate-smart forest management strategies that contribute to carbon neutrality on drained peat soils.

2 Material and methods

2.1 Model description

The simulation framework LandscapeDNDC (LDNDC) has been developed to allow a flexible problem-specific model composition for the simulation of the water, carbon and nitrogen cycles in cropland, grassland and forest ecosystems (Haas et al., 2013). In this study, the microclimate within the forests is simulated using the sub-model CanopyECM according to Grote et al. (2009). Vegetation related processes are modeled with the Physiological SImulation Model (PSIM) sub-model (Grote et al., 2006, 2011). Soil biogeochemical processes were represented with the $MeTr_x$ sub-model (Kraus et al., 2015), while soil hydrological conditions are represented with the Ecosystem Hydrology (EcHy) sub-model (Dirnböck et al., 2020).

PSIM enables the representation of a multiple species stand, where individual tree species can have their own characteristics and dimensions, while also having interactions with each other (Cade et al., 2021). Including multiple species in the simulation allows to consider the contributions of dominant trees, understorey and ground vegetation to carbon and water fluxes. In particular, the importance of understory in boreal forests has been highlighted before and is thus necessary to be included in the model (Korkiakoski et al., 2023; Leppä et al., 2020).

https://doi.org/10.5194/egusphere-2025-5197
Preprint. Discussion started: 30 January 2026

The soil sub-model MeTr$_x$ accounts for carbon and nitrogen pools and fluxes and their responses to land use and forest management. Most relevant processes considered by MeTr$_x$ for this study are humification, mineralization, nitrification and denitrification as well as CH_4 production and consumption (Kraus et al., 2015). In MeTr$_x$, various litter (Solutes, Cellulose and Lignin) and humus (Labile, Recalcitrant young and old) pools differentiated according to their chemical structure (Kraus et al., 2015) and carbon to nitrogen ratio, respectively. These are decomposed by microbial pools in the nitrification and denitrification processes. Besides pool size and matter properties, processes depend on the availability of oxygen, pH, clay content, and soil temperature and moisture. MeTr$_x$ also covers methane (CH_4) production as a final step at the end of decomposition under anaerobic conditions as well as CH_4 deposition. Oxygen content is dynamically calculated for each soil layer and as well as CH_4 oxidation. Detailed descriptions of these processes can be found in Kraus et al. (2015), Molina-Herrera et al. (2015), and Haas et al. (2022).

Soil water dynamics are calculated by the EcHy module, which predicts a dynamic groundwater table (z_{gw}) depending on the simulated water balance. In its conceptual design, EcHy is a one-dimensional (1-D) vertical soil column model. When applying its original version in this study, the simulation domain became waterlogged because precipitation exceeded evapotranspiration and percolation through the lower soil boundary. In reality, however, the site is drained by ditches that induce a lateral water flow component and counteract complete soil saturation. To account for this, a reference water table (Z_{gw}) was introduced, which represents the depth below which no significant lateral flow occurs (e.g., the ditch depth), and the soil is assumed to be fully saturated. In addition, a parameter representing lateral groundwater flow velocity and ditch distance Ψ was implemented. This parameter determines the rate of lateral water loss whenever the simulated dynamic water table depth z_{gw} is above Z_{gw}. Together, these modifications introduce a lateral (2-D) flow component into an otherwise 1-D framework, enabling EcHy to better reflect local site conditions. Lateral groundwater movement q is given by,

$$q = max(0.0, Z_{gw} - z_{gw}) \times \Psi \times K_s \tag{1}$$

z_{gw}: depth of groundwater, Z_{gw}: depth of reference groundwater, Ψ: Model parameter representing lateral groundwater gradient, K_s is the saturated hydraulic conductivity of the last soil layer. Negative Z_{gw}, z_{gw} means groundwater table is below soil surface.

Additionally, the size of the recalcitrant old humus pool ($H_{recalcitrant,old}$) was scaled as a function of the soil carbon to nitrogen ratio (C:N). The scaling factor was defined as,

$$s(C:N) = 0.8 - \frac{8}{C:N} \tag{2}$$

The scaling factor varies between 0 and 0.8. $H_{recalcitrant,old}$ is calculated as,

$$H_{\mathrm{recalcitrant,old}}(C:N) = \big(0.9 - s(C:N)\big) \times C:N \tag{3}$$

https://doi.org/10.5194/egusphere-2025-5197
Preprint. Discussion started: 30 January 2026

At low C:N ratios (nitrogen-rich soils), s(C:N) would be negative but the lower limit of scaling factor sets it to zero, resulting $H_{recalcitrant,old}$ would be approximately 0.9 * C:N. At high C:N ratios (nitrogen-poor soils), s(C:N) approaches 0.8 and is capped at this maximum, resulting in $H_{recalcitrant,old}$ to be approximately 0.1 * C:N. This formulation therefore reduces the size of the recalcitrant humus pool with increasing soil C:N ratio. Changes to the model code can be found Shahriyer et al. (2025c).

2.2 Site description

Lettosuo site, located in southern Finland ($60°38'31''$N, $23°57'35''$E), covers a total area of 65 ha (Fig. A1). The site, extensively drained in 1969 using ditches that were 45 m apart, is classified as a nutrient-rich Vaccinium myrtillus type II forest (MtkgII, Laine (1989)). Lettosuo was originally a sparsely treed, mesotrophic pine-birch sedge fen rich in herbs (Korkiakoski et al., 2023). Fertilizers were used after drainage to help with the growth of existing pine (*Pinus Sylvestris*) trees. In the 1970s and later, some thinning was done to ensure better growth of pine, but those thinning information are unavailable. Over time Lettosuo became a mixed forest site, where pine and birch (*Betula Pendula*) formed the overstory and spruce (*Picea Abies*) formed the understory canopy. The forest floor consisted of various herbs, shrubs and graminoids (Korkiakoski et al., 2023).

The site was divided into three sections according to the applied management methods: a control stand where no management action had taken place; a Continuous Cover Forestry (CCF) stand where all the pine trees (75 % of the original total biomass) were harvested in March 2016 (Korkiakoski et al., 2020); and a Rotational Forestry (RF) stand where all the trees were removed by clear-cutting, also in March 2016 (Korkiakoski et al., 2019).

In RF, the application of heavy harvesting machinery destroyed the ground vegetation, while in CCF, ground vegetation was only affected on logging trails. In RF, the harvest residues were left at the felling area, while in CCF, the harvest residues were placed on the logging trails. At RF, peat extracted from nearby ditches during ditch maintenance were used to form mounds of peat soil and new spruce seedlings were planted on top of the mounds in 2017. Most of the spruce seedlings died off during the drought in 2018 (Korkiakoski et al., 2023). Later as a result the stand became birch-dominated from the naturally occurring birch seedlings.

2.3 Site observations and auxiliary data

Finnish Meteorological Institute's long-term (1963-2021) observation-based meteorological data were used to drive the model (Aalto et al., 2016). Meteorological data consisted of temperature, precipitation, global radiation, wind speed and relative humidity. Nitrogen deposition in the form of ammonium and nitrate wet deposition was selected to match values (6 kg ha^{-1} y^{-1}) for the northern latitudes (Harmens et al., 2011). Background methane concentrations were set at a constant value of 1.74 ppb. RCP4.5 midyear CO_2 concentration was used for CO_2 concentration, which were gapfilled and bias-corrected towards observed CO_2 concentration.

One-sided Leaf Area Index (LAI) was estimated from Sentinel-2 satellite data for all stands and mostly consisted the post harvest years (Nevalainen, 2022; Korkiakoski et al., 2023). Additionally, the modeled pre-harvest LAI was compared against site estimated LAI reported by Leppä et al. (2020).

https://doi.org/10.5194/egusphere-2025-5197
Preprint. Discussion started: 30 January 2026

Table 1. Model soil layer setup, where soil depth in cm, Carbon (C) content, Nitrogen (N) content, Bulk density (BD), Carbon to Nitrogen ratio (CN), pH, Van Genuchten parameter n and (α), and minimum water filled pore space ($WFPS_{min}$) are given as,

Soil depth (cm)	C(%)	N(%)	BD	C:N	pH	n	α	$WFPS_{min}$
0-10	55	2.22	0.14	24.77	3.0	3.0	8.0	0.25
10-30	55	2.22	0.14	24.77	3.0	3.0	8.0	0.70
30-60	55	2.22	0.14	24.77	3.0	3.0	8.0	0.90
60-90	55	2.22	0.15	24.77	3.5	3.0	8.0	0.90
90-190	58	2.42	0.20	23.96	4.5	3.0	8.0	0.98

Data from the control stand included CH_4 fluxes, which were measured with six automatic chambers from June 2015 to January 2019. WT measurements at control stand covered the years 2016-2021 (Korkiakoski et al., 2020). The soil moisture content measurements at depths of 10 cm and 20 cm covered the duration from July 2015 to January 2019.

Eddy-covariance (EC) measurements of CO_2 exchange between the ecosystem and the atmosphere, i.e. net ecosystem exchange (NEE), were conducted on top of a telescopic mast (height 25.5 m until June 2019 and later at 27.2 m) at continuous cover stand. NEE before selective harvest will be referred to as pre-harvest and after selective harvest will be referred to as $CCF_{postharvest}$. The pre-harvest data covered the time period from January 2010 to March 2016 and $CCF_{postharvest}$ from April 2016 to December 2021. Gross primary production (GPP) and total ecosystem respiration (TER) were estimated from the NEE data (Korkiakoski et al., 2023) and used in this study to evaluate the LDNDC model performance. CH_4 measurements from the CCF stand were conducted with six automatic chambers from May 2015 to May 2018 (Korkiakoski et al., 2020), one year before the harvest and three years after the harvest. These were used to validate the CH_4 fluxes from CCF simulation. CCF also had continuous WT measurement from January 2010 to December 2021 (Korkiakoski et al., 2023).

A separate EC tower (height 3.2 m) in the rotational forestry stand was set up after the clear-cut harvest in March 2016 (Korkiakoski et al., 2019). NEE measurements from the RF after clear-cut, will be referred to as the $RF_{postharvest}$. NEE, GPP, TER and WT data from April 2016 to December 2021 were used in this study. CH_4 fluxes were measured with the manual chambers and covered the period of May 2016 to September 2017 (Korkiakoski et al., 2019).

2.4 Simulation setup

In the simulations, the vertical soil profile was divided into several layers of increasing thickness with increasing layer depth (Table 1). The carbon and nitrogen content, bulk density and pH of the soil layers were taken from the measured Lettosuo data previously reported by Leppä et al. (2020) and Korkiakoski et al. (2017). These soil variables and their prescribed initial levels are given in Table 1.

The simulations started from a pristine peatland condition in 1969. Fluctuations in litter and humus pools after initialization were stabilized during the first three simulation years. During this period, the Z_{gw} was set to 0.01 m depth to stabilize the soil carbon pools for pristine peatland condition. In the case of pristine peatland simulation, to study the soil carbon changes, the

https://doi.org/10.5194/egusphere-2025-5197
Preprint. Discussion started: 30 January 2026

Table 2. Individual species were introduced to the simulation starting from 1969. No species were removed for non-managed control and continuation of certain species until the end is indicated by –. Pine was removed for Continuous Cover Forestry (CCF) during selective harvest and all species were removed in the Rotational Forestry (RF) during clear-cut (RF_{CC}). Individual species were reintroduced for a new forest in RF ($RF_{Newforest}$) with number of seedlings $RF_{Newforest,n}$ reported in Korkiakoski et al. (2019).

Species	Initiation	Initial$_{n\ ha^{-1}}$	Control	CCF	RF_{CC}	$RF_{Newforest}$	$RF_{Newforest,\ n\ ha^{-1}}$
Pine	01/01/1969	535	–	01/03/2016	01/03/2016	01/04/2017	1520
Spruce	01/01/1972	1400	–	–	01/03/2016	01/04/2017	1120
Birch	01/01/1971	800	–	–	01/03/2016	01/01/2019	17400
Forest floor	01/01/1969		–	–	–	–	–

Z_{gw} was kept at 0.01 m until 2021. Otherwise, for forest stand simulations, Z_{gw} was set to 0.62 m after initial three years to represent drained peatland conditions. The model then simulated WT dynamically with the modification described in Section 2.1.

The initialization of tree species and forest floor vegetation is presented in Table 2. The simulation began in 1969 with pine trees and the forest floor vegetation. Birch and spruce were added in 1971 and 1972, respectively. Management events (selective harvest and clear-cut) took place in 2016. Harvest residues were left in the simulation domain and stemwood biomass was removed after management events. All simulations were run until end of 2021. All the modules were run with a sub-daily time step (30 minutes) and sub-daily and daily simulation outputs were used for various investigations.

The sensitivity of NEE to soil decomposition was tested (described in section 2.6 and Appendix A2) for a range of soil decomposition parameters (Table A1). Several of those sensitive soil parameters related to the decomposition of different humus and litter pools were later adjusted during forest stand simulations (Table A2). Species parameters reported in Grote et al. (2011), a study which simulated a mixed forest stand consisting of pine, spruce and birch trees on mineral soil in southern Finland, were used and adjusted to run the simulations for this study (Table A2). These parameters included e.g. photosynthesis related VCMAX (Maximum RubP saturated rate of carboxylation at 25°C for sun leaves), KM20 (Maintenance coefficient at reference temperature), SLAMAX (Specific leaf area in the shade) and SLAMIN (Specific leaf area in the full light).

2.5 Model data analysis and evaluation

The correlation coefficient (r) and Nash-Sutcliffe efficiency (NSE) were calculated from the daily aggregate of the available measurements and corresponding modeled data. NSE values can vary from $-\infty$ to 1. Model output that produces an NSE value of 1 is described as the perfect simulation. Preferably NSE values greater than 0.5 are desirable, indicating good model performance.

NSE is defined as,

https://doi.org/10.5194/egusphere-2025-5197
Preprint. Discussion started: 30 January 2026

$$NSE = 1 - \frac{\sum_{i=1}^{n} (Q_{o_i} - Q_{m_i})^2}{\sum_{i=1}^{n} (Q_{o_i} - \overline{Q_o})^2} \quad (4)$$

Where, Q_o represents the observed data at time i, Q_m represents the modeled data at time i, $\overline{Q_o}$ is the mean of the observed data. n is the total number of observations.

We further used Root Mean Square Error (RMSE) to quantify the differences in NEE and WT between the model and the observations. In this analysis, seasons are defined as December–January (winter), March–May (spring), June–August (summer) and September–November (autumn).

Since a single simulation setup was used for all three forest stand simulations before the harvesting events, both measured and simulated data will be referred to as pre-harvest data (2010–2015). Korkiakoski et al. (2023) calculated the Annual CO_2 balances (NEE, GPP and TER) for 2016 from April 2016 to March 2017 and the modeled estimates for 2016 was also calculated similarly in the $CCF_{postharvest}$ and $RF_{postharvest}$. To show the sensitivity of the simulated CH_4 flux with WT after clear-cut harvest, the groundwater lateral gradient parameter was changed (28.7 to 38.7, Table A2) in the simulation to reproduce the lowest and highest observed WT at RF (section 3.3).

The effect of drainage on the simulated soil carbon (SC) storage was compared to the SC loss reported by (Simola et al., 2012). The influence of harvesting, under different management methods, on SC dynamics was assessed by quantifying changes in SC following harvest. This included investigating the partition of different litter (solutes, cellulose and lignin) and humus (labile, recalcitrant young and old) pools. The evolution of the total carbon (soil carbon + carbon in vegetation) over the whole simulation period was also studied (section 3.5). A pristine peatland simulation, without any drainage or harvesting, served as a reference. Data and pyhton codes used in this study can be found from Shahriyer et al. (2025a).

2.6 Sensitivity test

Sensitivity tests for soil parameter were carried out separately with mature forest stands in 1-year simulation runs. Soil parameters and their range selected for the sensitivity tests are given in Table A1. The fixed species parameters used in the sensitivity tests are given in Table A2. For sensitivity testing, the Python library SPOTPY and its FAST algorithm was used (Houska et al., 2015, 2017). Soil parameters were separated into three sets, each consisting of nine parameters (Table A1). The sets consisted of decomposition constants for different soil pools, factors related to dependency on conditions for decomposition and factors related to the humification of different soil pools. With this setup, the simulation was run 8649 times (Houska et al., 2017) for each set of parameters, and the soil parameter values were randomly selected by the FAST algorithm. FAST algorithm indicates the sensitive parameters in the parameter sets.

First, sensitivity among the parameters related to the decomposition was tested. Further, to proceed from one set of parameters to the next, we compared the simulation output of NEE from the sensitivity test runs with measured NEE values. Within the range of minimum and maximum parameter values, the parameter value that produced the best NSE was selected and subsequently used as fixed parameter values for first set of soil parameters when the next set of nine soil parameters was run. A similar procedure was followed for the third parameter set. The results of these tests are given in the Appendix (Fig. A2-4).

https://doi.org/10.5194/egusphere-2025-5197
Preprint. Discussion started: 30 January 2026

Table 3. Comparison between simulated vegetation structure with observations before management at stand age of 45 years (08/2014). Simulated outputs are shown in bold. Tree numbers (n ha^{-1}), tree heights and stand volumes collected (Korkiakoski et al. (2023)) from Lettosuo site are given in parenthesis. SD is the standard deviation. Simulated individual tree species diameters are given in bold. LAI estimates for individual species reported by Leppä et al. (2020) are given in parenthesis.

Vegetation	Trees (n $ha^{-1} \pm$ SD)	Height (m)	Volume ($m^3 \pm$ SD)	Diameter (cm)	LAI (m^2 m^{-2})
Pine	**488** (494 ± 11)	**17.1** (20)	**203** (184 ± 13)	**25.2**	**1.80** (1.92)
Birch	**733** (765 ± 32)	**13.2** (13)	**38** (52 ± 1)	**9.8**	**1.19** (1.12)
Spruce	**1285** (1252 ± 80)	**8** (7–10)	**30** (32 ± 11)	**7.8**	**1.69** (1.62)
Forest floor	–	–	–	–	**0.94** (1)

The parameter related to the decomposition of recalcitrant young humus was the most sensitive in the first set of sensitivity tests (Fig A2). Other sensitive parameters in this set were related to the decomposition of labile humus, recalcitrant old humus, raw litter and the dependence of decomposition on litter lignin concentration. In the second set of parameters, parameters related to temperature, pH and decomposition reduction due to anaerobicity were found to be sensitive (Fig. A3). The parameters related to C:N ratio of the old humus pool to the total soil C:N ratio, the humification of the recalcitrant young humus, dissolved organic carbon, active organic material and solutes were the most sensitive parameters in the third set (Fig. A4).

According to the results of the parameter sensitivity tests, parameters related to the temperature dependency of decomposition, decomposition of raw litter and wood, decomposition constants for three humus pools. Their values are given in Table A2.

3 Results

3.1 Development of forest structure before and after management

In the forestry stand simulations, the simulated forest stand at age 45 showed the number of trees of individual species was within the range of observations (Table 3). The height of the individual species was also close to the observed values. The modeled pine and spruce volumes were close to the range of observed volumes, while birch had 27% less volume. Modeled LAI of different species matched well with reported LAI before harvest in 2014 (Fig. 1a). The modeled LAI of 0.94 m^2 m^{-2} for forest floor vegetation in August 2014 was similar to the LAI of 1 m^2 m^{-2} reported by Leppä et al. (2020). The same literature reported LAI for above ground canopy (pine + spruce + birch) to be 4.66 m^2 m^{-2} and the corresponding modeled LAI was 4.68 m^2 m^{-2} (August 2014; Table 3).

Modeled pine and spruce LAI were diminishing from 2016 to 2021 for control simulation (Fig. 1b), which was not seen in the prior six years (Fig S1). The sum of pine and birch modeled LAI was closest to the satellite-based LAI (Fig. 1b), and this could be realistic since pine and a small percentage of birch were forming the upper-story canopy in the control stand. The

https://doi.org/10.5194/egusphere-2025-5197
Preprint. Discussion started: 30 January 2026

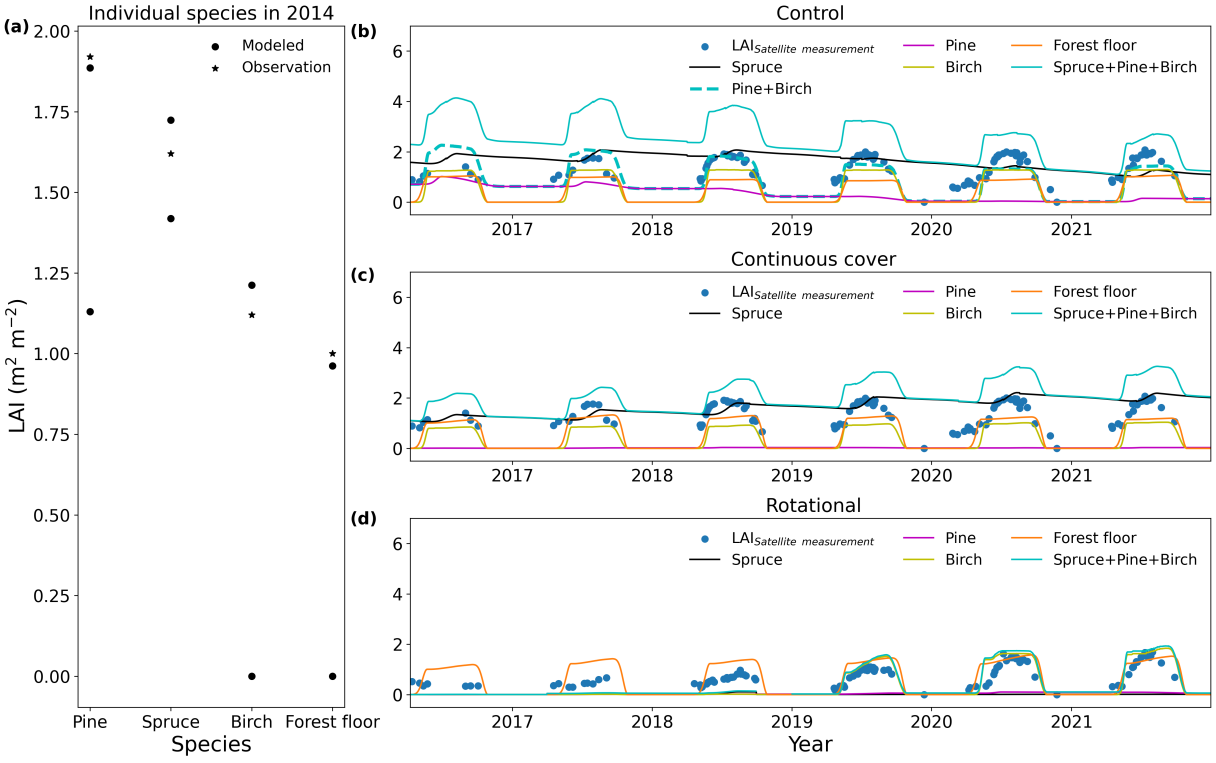

Figure 1. (a) Comparison of individual species one-sided Leaf Area Index (LAI) estimates from field observations (stars) (Leppä et al., 2020) with minimum and maximum modeled LAI (circles) in 2014 for a 45-years-old forest. **(b)**, **(c)** and **(d)** show LAI development in different management scenarios and one-sided LAI comparisons between the model (solid and dashed lines) and satellite-estimated LAI (blue dots). The Pine+Birch LAI only for the control **(b)** are shown with dashed lines.

250 decrease in LAI was not seen in the CCF simulation because of the removal of the pine during harvest and infect spruce LAI was increasing up to 2021 (Fig. 1c). Spruce LAI during summer months was closer to satellite-based LAI, while the sum of spruce and birch modeled LAI was always larger than the satellite-based LAI (Fig. 1c). The modeled LAI for birch and forest floor remained consistent from 2016 to 2021 for both control and CCF. After clear-cutting in RF, the modeled LAI was almost double the satellite-based LAI in 2016, whereas the discrepancy between the two decreased progressively after 2018 (Fig. 1d).
255 Simulated birch and forest floor LAI were closest to satellite-based LAI in 2019 to 2021 (Fig. 1d).

3.2 Dynamics of soil moisture, water table

Soil moisture dynamics were simulated well for 2015–2017 (May - September), but there were some differences between the model and measurements in 2018 (Fig. 2). The model captured the dynamics of 10 cm soil moisture for 2016 and 2017 best. However, in 2015, the model 10 cm soil moisture was slightly lower compared to the measurements and in 2018, the modeled

https://doi.org/10.5194/egusphere-2025-5197
Preprint. Discussion started: 30 January 2026

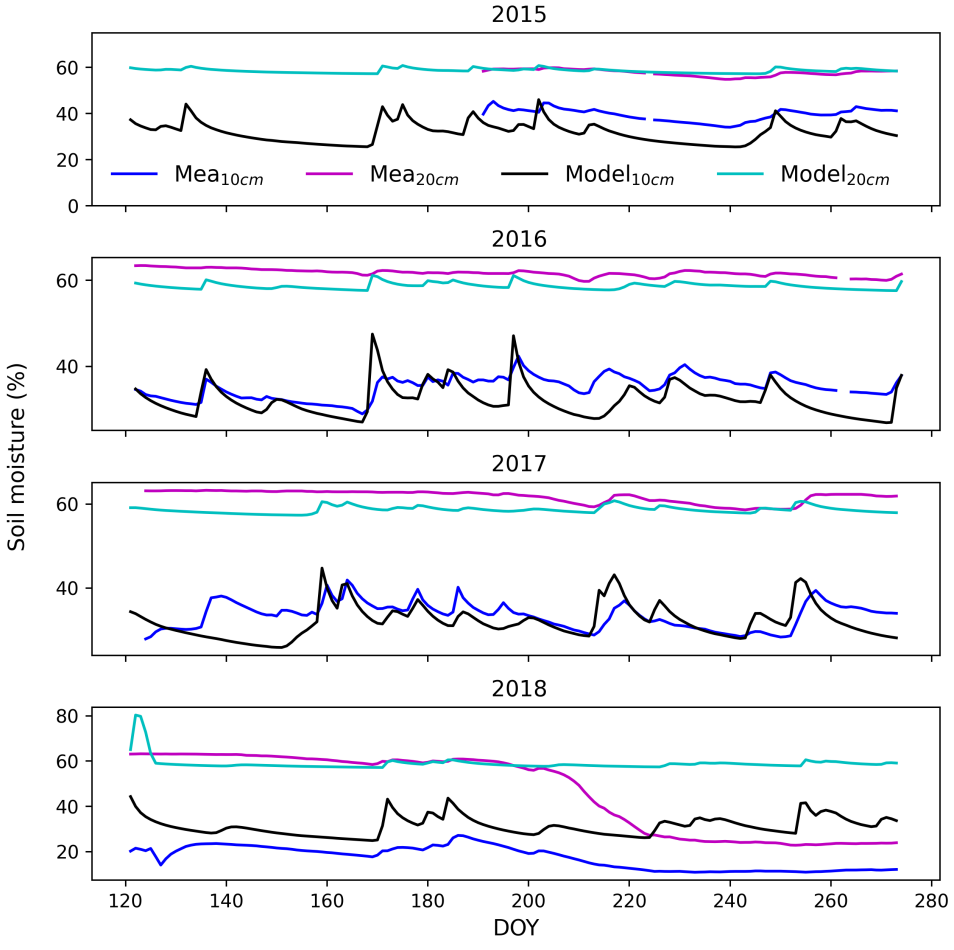

Figure 2. Simulated and measured soil moisture for the control stand from the beginning of May to the end of September shown in day of year (DOY). Blue and magenta lines show measured soil moisture at 10 and 20 cm depths, respectively. Black and cyan lines show the simulated soil moisture at 10 and 20 cm depths, respectively.

10 cm soil moisture was higher compared to the measurements. For 20 cm depth, the model produced the best results for 2015–2017 but from July 2018 onward, model overestimated the soil moisture.

The modeled WT in the pre-harvest years (2010-2015) were similar to the observations conducted at the CCF stand (Fig. 3a). The simulation showed large deviations from the measured mean in especially during summer and autumn in 2016 and 2017 (See also Fig. S2). From 2018 onward the modeled WT in CCF stand was again similar to the observed WT. The model also predicted the control stand WT within the observed range and reflected the observed dynamics (Fig. 3b). The largest

https://doi.org/10.5194/egusphere-2025-5197
Preprint. Discussion started: 30 January 2026

differences in the control stand occurred in the autumn in 2018 and 2019 (See also Fig. S3). WT comparison between the model and observations at the RF stand also showed that the simulated WT following the observed dynamics (Fig. 3b) had much lower differences between model and measured WT (Fig. S4). Modeled WT rises after clear-cut at RF stand, while rise in WT from selective harvest at CCF stand was not significant (Fig. S5).

3.3 Methane flux comparison and sensitivity with water table

Manual chamber measurements showed RF stand to be a source of CH_4 in summer months after clear-cut harvest. As the simulations originally showed CH_4 sink for the same period, the role of WT on the difference was further investigated. Indeed, the CH_4 flux in the model was found to be sensitive to the WT variations after clear-cut. The groundwater lateral gradient parameter was modified to simulate WT similar to the lowest and highest observed WT at the RF stand in two RF simulations (Fig. 4). In these simulations, simulated WT were similar before the clear-cut but changed after the clear-cut. No additional changes were needed for the model setup to produce the shift in WT. Simulation with the original value of groundwater lateral gradient parameter, that produced the lowest WT, led to a higher sink of CH_4. While the modified parameter value produced a higher WT and resulted in smaller sink of CH_4. In high WT simulation, the site was even a source of CH_4 on some occasions. Both RF simulations showed very little changes in modeled CH_4 fluxes before harvest and the model simulated a lower CH_4 sink compared to the measurements (Fig. 4).

Modeled CH_4 flux was within the variation of the automatic chamber measurements for both control and CCF stand (Fig. 5). The measurements showed mostly uptake of CH_4 from the atmosphere over the 3.5 years of measurements at both stands. When looking at the seasonal dynamics, compared to the measurements, the model was in the upper end of CH_4 uptake during spring and summer, while the model underestimated the uptake during autumn and early winter. However, the underestimation of uptake was not clearly evident in 2016 for either stand.

3.4 Ecosystem CO_2 exchange before and after management

The model captured the NEE better in the pre-harvest simulation (r = 0.88, NSE = 0.75, slope = 0.92) than in either $CCF_{Postharvest}$ and $RF_{Postharvest}$(Fig. 6a - c). Performance for modeled GPP was similar for both pre-harvest and $CCF_{postharvest}$, while $RF_{postharvest}$ had a lower NSE (0.75) and higher slope (1.26) to the fitted line (Fig. 6d - f). A similar comparison for TER showed that the modeled TER performed well in all three simulations (r = 0.94 - 0.96, NSE = 0.87 - 0.92, Fig. 6g - i). The complete daily time series with gapfilled measurements and model results are given in supplementary section 3 (see also Fig. S6-11 and Fig. S12 for a half hourly comparison).

On the annual scale, the modeled NEE (NEE_{Mod}) was similar to the EC-measured NEE (NEE_{EC}) in both pre-harvest and post-harvest conditions with some exceptions. The largest discrepancy in NEE_{Mod} was seen in 2014 followed by 2012 during pre-harvest years (Fig. 7a), and first post-harvest year (4/2016 - 3/2017) of both CCF (Fig. 7b) and RF (Fig. 7c). In $CCF_{postharvest}$, NEE_{Mod} was a net source of CO_2 for the first three years after selective harvest, similar to the NEE_{EC}. NEE_{Mod} was a sink of CO_2 from the fourth year onward, same as the NEE_{EC}. In the $RF_{postharvest}$, the NEE_{Mod} was a source

https://doi.org/10.5194/egusphere-2025-5197
Preprint. Discussion started: 30 January 2026

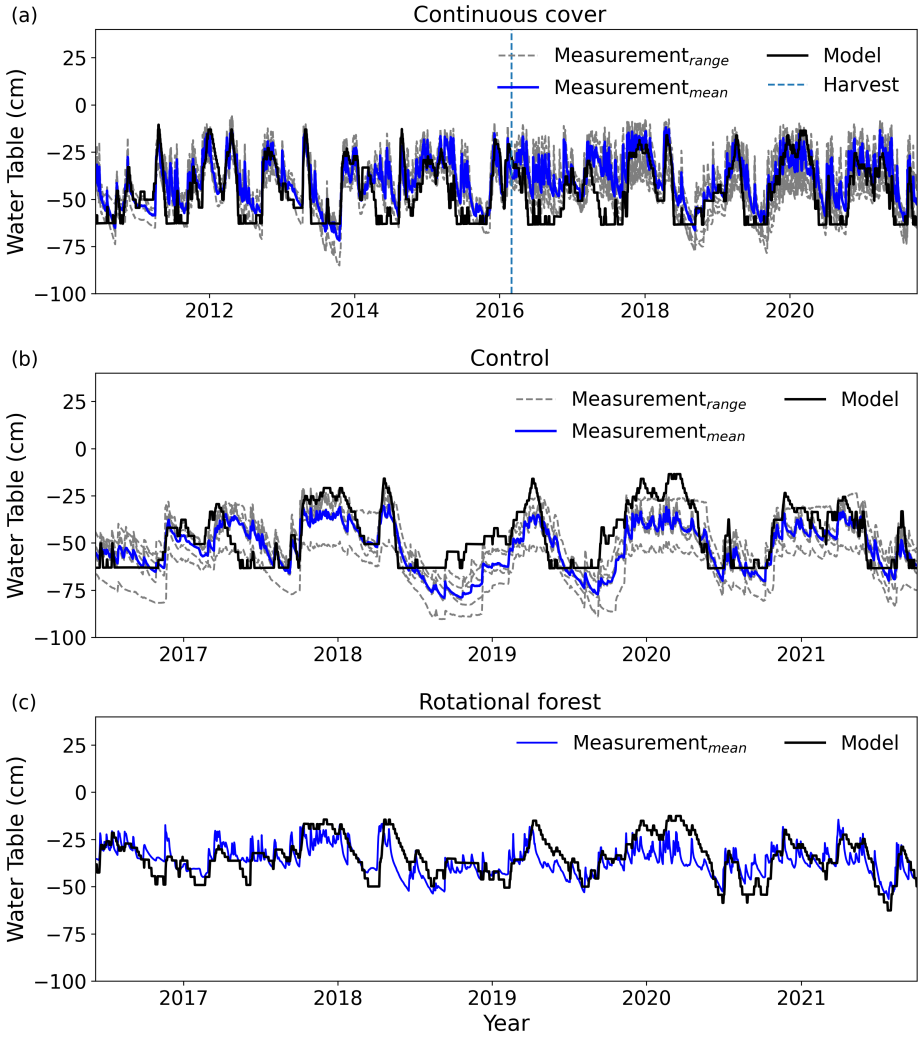

Figure 3. Water table (WT) dynamics in the **(a)** continuous cover forestry stand (CCF, includes pre-harvest and post-harvest WT), **(b)** control stand and **(c)** rotational forestry stand. Blue and black lines represent the mean measured and simulated WT depth, respectively. Gray dashed lines show the range of measured WT from different WT loggers at the CCF and control stand. The blue vertical dashed line shows when the selective harvest took place at the CCF stand. Negative values represent WT below the soil surface.

of CO_2. NEE_{Mod} is similar to the NEE_{EC} for the six post-harvest years after clear-cut. Both modeled and observed annual ecosystem CO_2 emissions decreased over time after the clear-cut.

https://doi.org/10.5194/egusphere-2025-5197
Preprint. Discussion started: 30 January 2026

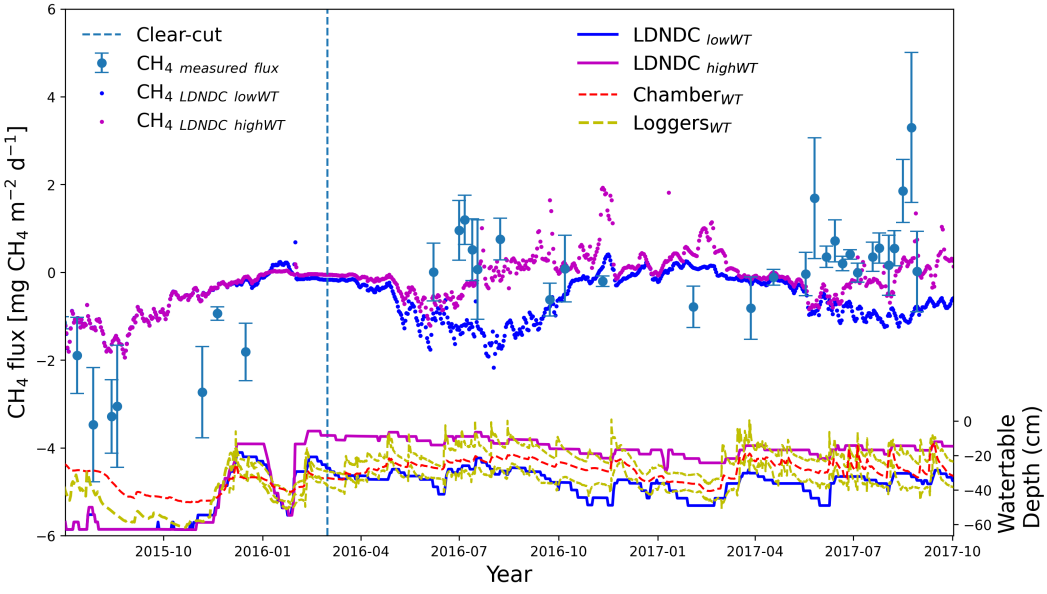

Figure 4. Manual chamber CH_4 flux measurement is represented by light blue dots and associated standard deviation shown with the bars. The highest and lowest Water Table (WT) observed from automatic WT loggers at the rotational forestry (RF) stand are shown in yellow dashed line. WT measured along manual chamber is given in red. Low and high-WT, simulated by modifying groundwater lateral gradient parameter, shown at the bottom by darker blue and magenta, respectively. Corresponding modeled CH_4 fluxes are shown at the top with darker blue and magenta dots, respectively. Vertical dashed blue line shows the timing of the clear-cut harvest at RF.

In the pre-harvest, modeled GPP (GPP_{Mod}) was similar in magnitude to the EC based GPP (GPP_{EC}) and the biggest difference was in 2014, when GPP_{Mod} was 35% higher (Fig. 7d). In the $CCF_{postharvest}$, GPP_{Mod} had a similar pattern compared to the GPP_{EC} and the largest difference taking place in 2018, when the GPP_{Mod} was 44% higher than the GPP_{EC} (Fig. 7e). In the $RF_{postharvest}$, the GPP_{Mod} ranged from 21% lower (2018) to 24% higher (2021) compared to the GPP_{EC} (Fig. 7f). In the pre-harvest condition, modeled TER (TER_{Mod}) and EC-based TER (TER_{EC}) did not show much difference in the balances (Fig. 7g). In $CCF_{postharvest}$, TER_{Mod} was higher in 2018 (28%) and 2019 (26%) (Fig. 7h), and in $RF_{postharvest}$, TER_{Mod} ranged from 16% lower (2017) to 22% higher (2021) compared to the TER_{EC} (Fig. 7i).

3.5 Management effect on soil carbon storage

Simulated SC storage started to decrease after drainage and continued until the management events (Fig. 8). In contrast, pristine peatland with no drainage showed a small accumulation of SC assuming a conservative ground vegetation coverage of 40% of the area. The development of SC after the harvest varied among the managements and depended on the management method. In control, where no trees were removed, SC continued to decrease until the end of the simulation. In CCF, where the forest was partially removed, SC accumulated for a couple of years likely due to the carbon input from harvest residue, after which it started to decrease again, although SC remained higher than in control. In RF, where all trees were removed, the SC increased

https://doi.org/10.5194/egusphere-2025-5197
Preprint. Discussion started: 30 January 2026

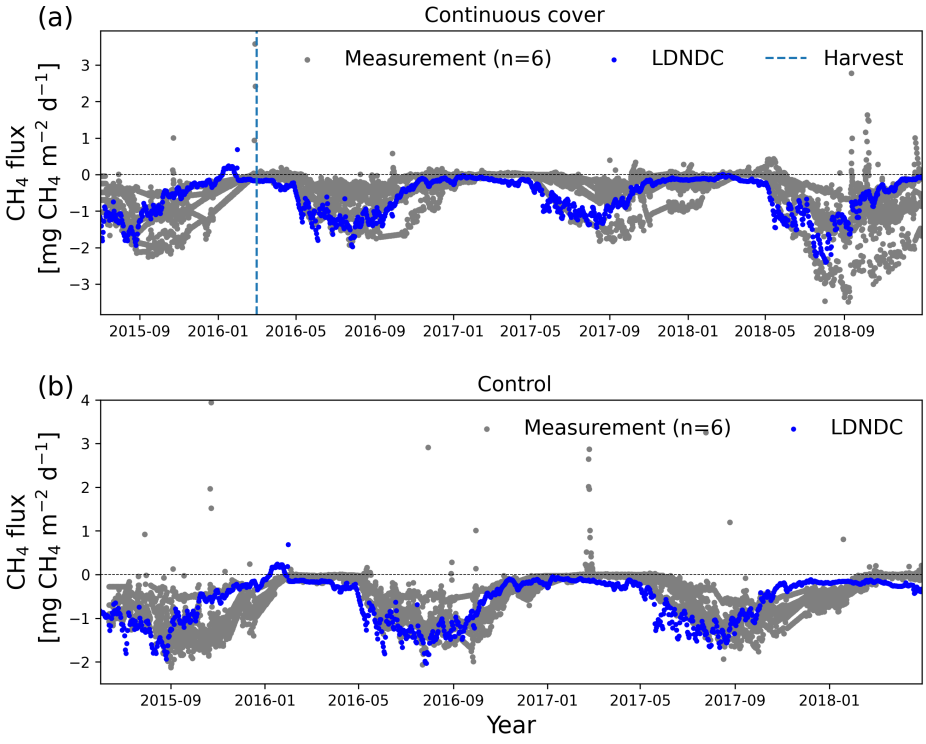

Figure 5. Time series of modeled (blue) CH_4 flux and 6 automatic chamber measurements (gray, n=6) conducted at the **(a)** continuous cover forestry (CCF) and **(b)** control stand. Vertical dashed blue line in **(a)** shows the selective harvest at CCF.

for few years likely due to the carbon input from harvest residue and then started to decrease, but SC remained higher than in both control and CCF. Annual SC loss for 2010–2015 period was 233 g C m^{-2} y^{-1}. SC loss for 03/2016–2021 period was 221 g C m^{-2} y^{-1} in control, 95 g C m^{-2} y^{-1} in CCF, and SC gain 79 g C m^{-2} y^{-1} in RF.

The difference between total carbon (TC) and SC in pristine was small and owing to a relatively small amount of carbon stored in the vegetation (Fig. 8). After the drainage, TC decreased for all forestry simulation scenarios since there was more carbon lost from the soil compared to the carbon accumulated by the vegetation. With continued forest growth, trees accumulated more carbon, and TC leveled off between 2000–2010 and showed an upward trend in that time as vegetation carbon uptake exceeded SC loss. In control, TC continued to increase until the end of the simulation. However, in CCF, TC decreased for a few years after the selective harvest and once the remaining vegetation rebounded TC started to increase again. In contrast, in RF, the accumulation of carbon by the forest stopped after the mature forest had been removed. Also, the newly planted forest was not accumulating enough carbon to offset the carbon lost from the soil, resulting in a downward trend in TC.

https://doi.org/10.5194/egusphere-2025-5197
Preprint. Discussion started: 30 January 2026

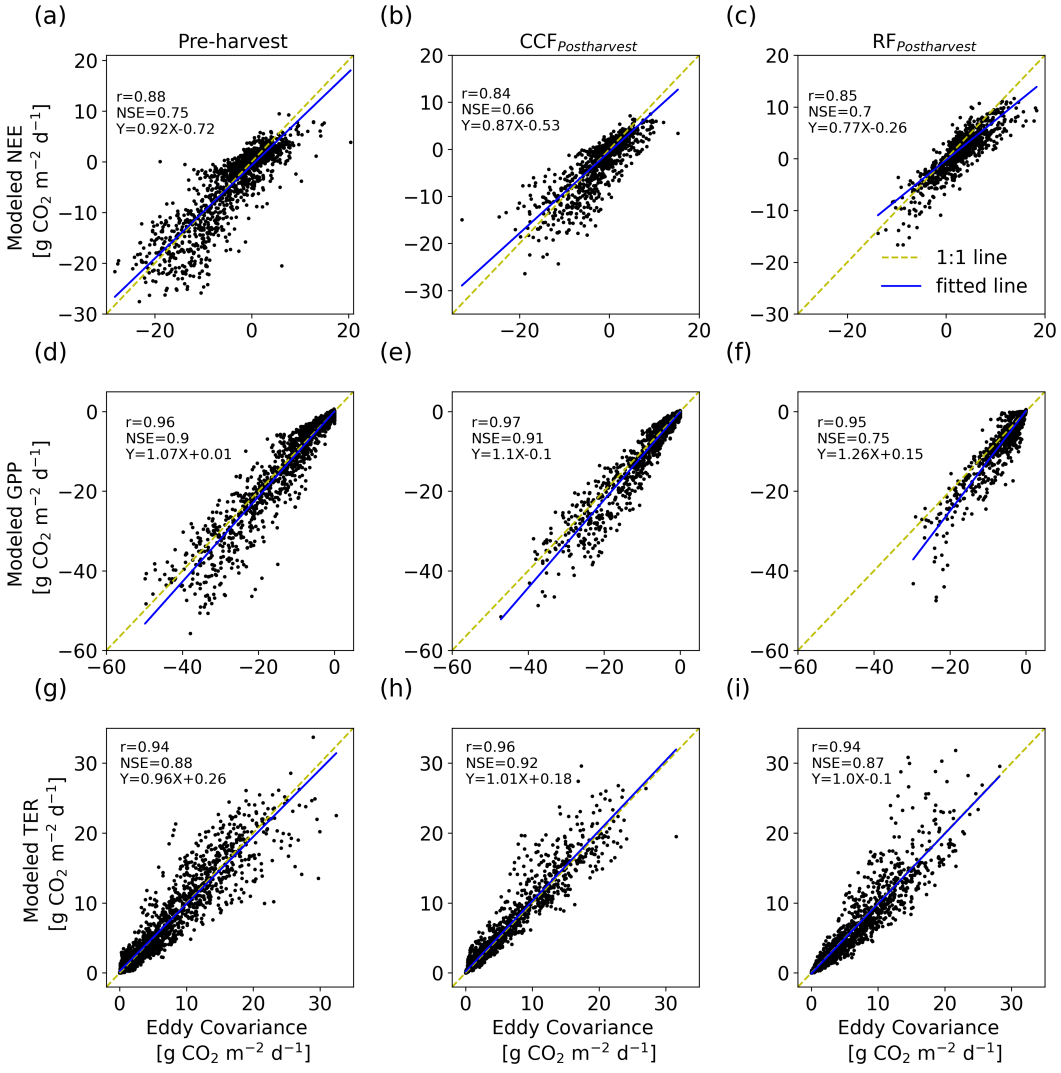

Figure 6. Modeled versus measured NEE (a-c), GPP (d-f) and TER (g-i) for pre-harvest (a, d, g) and post-harvest conditions of the continuous cover forestry (CCF; b, e, h) and rotation forestry (RF; c, f, i) stand. Correlation coefficients (r) and Nash–Sutcliff model efficiency (NSE) given in the figures show agreement among the variables compared. Yellow dashed lines and blue lines are the 1:1 lines and fitted lines, respectively. The equations for fitted lines are given as Y. For this comparison, the instances when measurement data were missing, the corresponding modeled time periods were removed and then daily sums were taken for both.

https://doi.org/10.5194/egusphere-2025-5197
Preprint. Discussion started: 30 January 2026

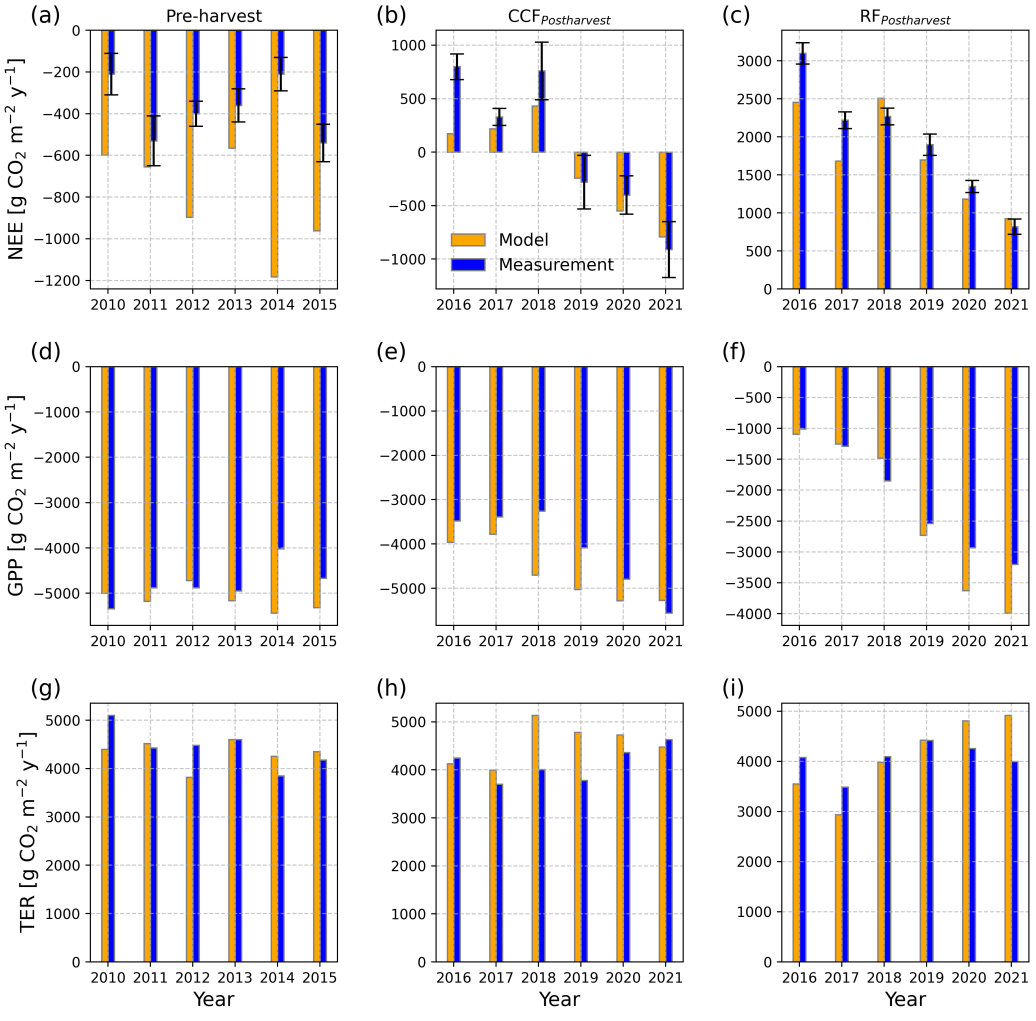

Figure 7. Annual balances of modeled net ecosystem exchange (NEE) and EC-based NEE (gapfilled) for pre-harvest, CCF$_{postharvest}$ and RF$_{postharvest}$ shown with the subplots **(a)**, **(b)** and **(c)**, respectively. Uncertainties in the EC-based NEE (Korkiakoski et al., 2023) are shown with the error bars. Similarly, pre-harvest, CCF$_{postharvest}$ and RF$_{postharvest}$ gross primary product (GPP), are shown in **(d)**, **(e)** and **(f)** and total ecosystem respiration (TER), are shown in **(g)**, **(h)** and **(i)**, respectively. Negative values represent uptake by the ecosystem and positive values represent release of CO_2 to the atmosphere.

https://doi.org/10.5194/egusphere-2025-5197
Preprint. Discussion started: 30 January 2026

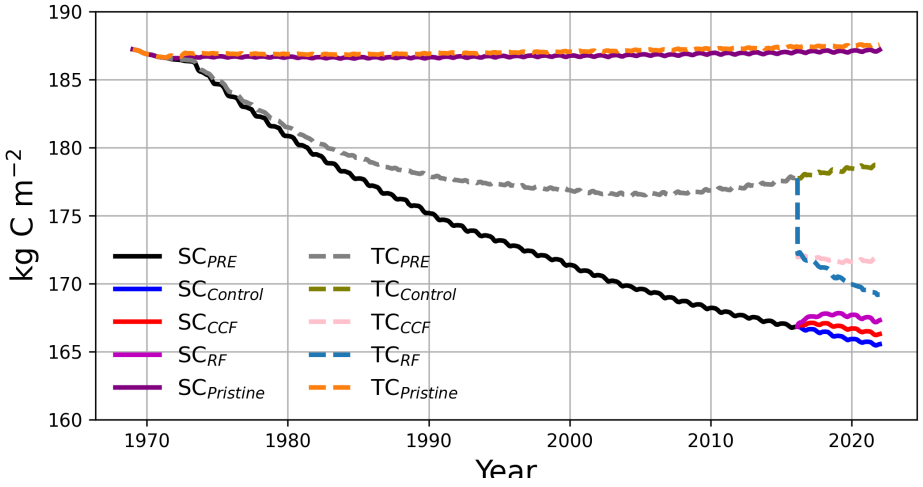

Figure 8. Modeled soil carbon (SC, solid lines) and total carbon (TC, dashed lines) time series for the different simulations from 1969 to 2021. Purple and orange show SC and TC for non-drained pristine peatland. Black and gray show the SC and TC development up to the harvest event in March 2016, respectively. Blue, red and magenta show the SC development for control, continuous cover forestry (CCF) and rotational forestry (RF) scenarios after harvest, respectively. Olive green, pink and light blue represent TC for control, CCF and RF scenarios after the harvest, respectively.

The litter pool (solutes) with a fast turnover rate had a high initial input from harvest, but the amount of solutes decreased very fast (Fig. 9a). After the initial spike, the solutes at RF were even lower than that of control and CCF in 2016-2019 since the remaining vegetation was not producing fresh litter. That rebounded once the birch started to influence the litter input from the fourth year after clear-cut. For both CCF and RF, cellulose and lignin litter pools dominated the total litter pool, while solutes contributed comparatively little (Fig. 9b and c). Cellulose litter pool reached its peak in the third (RF) and second (CCF) year after the harvest and started to decrease after that, while the lignin litter pool started to decrease on the fourth year of harvest.

There was also an initial increase to the storage of fast decomposable labile humus pool after the harvesting events as a result of input from freshly decomposed harvest residue (Fig. 9d). The peak in the labile storage was reached earlier in RF compared to CCF. Contribution of decomposed harvest residue to the labile humus pool was larger in RF than CCF. The decomposed harvest material also affected the recalcitrant young humus pool (Fig. 9e). A minimal effect on the recalcitrant old humus pool was seen after harvest from simulation (Fig. 9f).

4 Discussion

LDNDC model simulated the forest structure realistically with the prescribed species composition for a drained forested peatland before and after the management events. Comparing modeled LAI with field estimated LAI reported by Leppä et al. (2020) showed similar LAI values in a mature forest. But the sum of the modeled LAIs of all the individual tree species did not

https://doi.org/10.5194/egusphere-2025-5197
Preprint. Discussion started: 30 January 2026

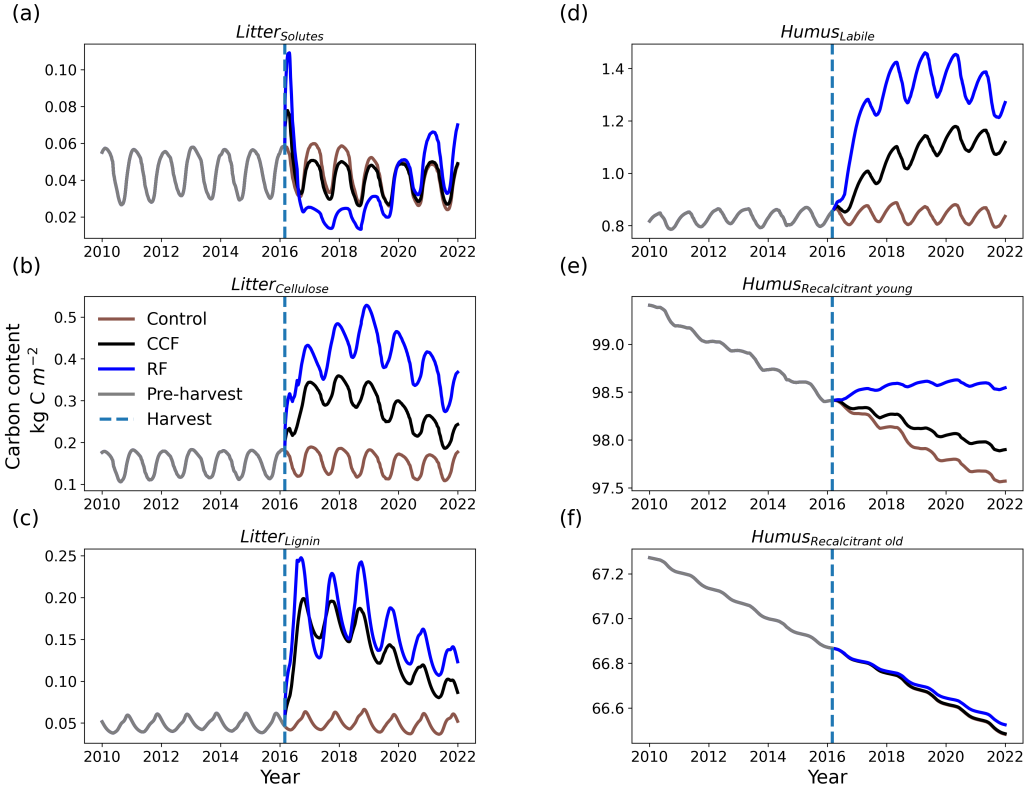

Figure 9. Litter (a, b and c) and humus (d, e and f) pools during pre-harvest and post-harvest conditions. Pre-harvest is shown in gray, control in brown, Continuous Cover Forestry (CCF) in black and Rotation Forestry (RF) in blue. Dashed light blue line shows the harvesting time.

gave the same perspective as satellite estimated LAI. This could be because the satellite estimated LAI most likely reflects the status of primary canopy of pine and birch at the study site. The control stand had a dense canopy (Fig. A1) and the visibility of the secondary vegetation and forest floor can be poor with the satellite. Modeled LAI matched with the satellite-estimated LAI well for CCF and RF stands after management because vegetation was sparse at the CCF stand immediately after selective harvest and almost no vegetation at the RF stand after clear-cut (Fig. A1). So model comparison with satellite estimate for these sparse vegetation stands gives much more accurate picture. Further, the declining trend in the modeled LAI for pine and spruce in control stand could be a result of competition between species.

The model captured the temporal dynamics of the WT well and in the simulations the fluctuations in WT at the RF were more pronounced compared to the CCF, where fluctuations were hard to distinguish. Fluctuations in the WT due to management had been reported for the Lettosuo site from previous field studies (Leppä et al., 2020; Korkiakoski et al., 2019, 2020) and suggested an increase of 18-23 cm in WT at RF. The simulated WT could not get below the prescribed Z_{gw} of 0.62m, which in turn have

https://doi.org/10.5194/egusphere-2025-5197
Preprint. Discussion started: 30 January 2026

contributed to the trees not suffering from any drought effect in the simulations. As water was always available for the trees to uptake, this fact could explain why the effects of drought on CO_2 balance in summer 2018 (Korkiakoski et al., 2023) were not captured by the model when daily time series was investigated. But in annual scale for both CCF and RF the discrepancies in CO_2 balance in 2018 was not large even though 2018 was exceptionally dry (Lehtonen and Pirinen, 2019). This suggests that water availability below Z_{gw} for roots had only a minor influence in the overall CO_2 balance.

The simulation of the CH_4 fluxes for control and CCF was good, and the site was mostly a sink of CH_4. However, CH_4 flux dynamics after clear-cut in the RF were quite sensitive to the changes in WT. According to the measurements, RF changed from CH_4 sink to source after clear-cut (Korkiakoski et al., 2019). However, the model was showing the RF to be a sink of CH_4 after the clear-cut in the RF simulation with low WT, and a season-dependent source and sink in the RF simulation with high WT . Another measurement study with two different RF sites showed that the sites remained small sinks (0.07 and 0.52 mg CH_4 m^{-2} d^{-1}) of CH_4 even after clear-cut (Huttunen et al., 2003). CH_4 flux could be dependent on the localized WT . Thus, the placement of the chambers compared to the distance of ditches is an important factor to consider when comparing the model results with measurements (e.g., Laurén et al., 2021). The locations for the manual chambers in this study varied within 4–22.5 meters from the ditch and here we used an average WT from the chambers. Additionally, logger WTs were included in the study to cover the variability in the study site.

The simulated CO_2 annual balances showed net CO_2 sink similar to the observation for the pre-harvest period. Also, the simulated CO_2 annual balances for $CCF_{postharvest}$ and $RF_{postharvest}$ were in good agreement with the measurements in terms of when the stand (CCF) became a sink after harvest or how long the stand (RF) stayed a source. In CCF, after selective harvest, the annual balance had a similar trend for both observation and simulation, where the first three years were a source of CO_2 and the next three years were a sink. However, we saw a small increase in the modeled GPP and TER already on the third year after the harvest, which was not evident in the observation-based GPP and TER. This could suggest that the simulation overestimates the recovery speed of the vegetation. In RF, after the clear-cut, the ecosystem was a source of CO_2 to the atmosphere according to both model and observations, which is largely due to the removed assimilation capacity of trees and increasing respiration from the harvest residuals. Korkiakoski et al. (2019) reported the contribution from the harvest residue to the TER after clear-cut. The underestimation in the NEE for first two years after clear-cut resulted from the model estimate of TER being lower compared to observations.

In this study the simulated annual soil carbon loss was -421 g C m^{-2} y^{-1} over 30-years period (1980-2009). A study by Simola et al. (2012), where 37 samples from peat sites with different fertility types from all over Finland were taken during the same time period, reported a minimum carbon loss from the drained peatland soil to be around -150 g C m^{-2} $year^{-1}$. Soil carbon loss at a fertile drained peatland site in southern Finland can even be around -1000 g C m^{-2} y^{-1} (Ojanen et al., 2013). Our study site is a MtkgII type peatland forest (Vasander and Laine, 2008). Different drained sites with the MtkgII status could have varying amounts of carbon loss from peat, which is regulated by WT and temperature (Ojanen et al., 2013). Thus the soil carbon loss from the simulation was in acceptable range when compared to the literature. The slowdown in SC loss for CCF and SC gain in RF compared to continuous SC loss in control was due to the large input of carbon from fresh litter and harvest residue into the soil. The residue contribution was larger in RF compared to CCF, resulting in the SC storage gaining more

https://doi.org/10.5194/egusphere-2025-5197
Preprint. Discussion started: 30 January 2026

carbon in RF. Higher WT in the RF could also affect soil carbon storage, resulting in reduced carbon loss from soil. SC storage started to decrease again at the RF already from the fourth year after the harvest and for CCF even earlier as input from the decomposition of harvest residue started to diminish. Also the lowering of WT because of the increased transpiration from the growing vegetation started to contribute to the SC loss.

5 Conclusions

The process-based LandscapeDNDC model was successfully applied to simulate forest development under different managements on drained peatland from seedlings to maturity. The simulations demonstrated that estimates of carbon fluxes and the overall greenhouse gas balance vary substantially depending on management type, underscoring the importance of detailed information on management history, tree dimensions, and regrowth dynamics. The model reproduced measurement-derived NEE, GPP and TER both before and after harvest, while also capturing changes in forest structure. The implementation of a new dynamic water table (WT) module improved simulations of WT level, soil moisture, peat decomposition, and CH_4 fluxes, thereby enhancing the representation of carbon dynamics. We were able to illustrate the contributions of harvest residue to litter and humus pool and their decomposition. This successful application of LandscapeDNDC provides a robust basis for investigating future management scenarios in drained peatland forests, with respect to both carbon and energy balances. The model therefore offers valuable insights for developing forest management strategies that supports climate neutrality in peatland ecosystems.

https://doi.org/10.5194/egusphere-2025-5197
Preprint. Discussion started: 30 January 2026

Appendix A

A1 Lettosuo site

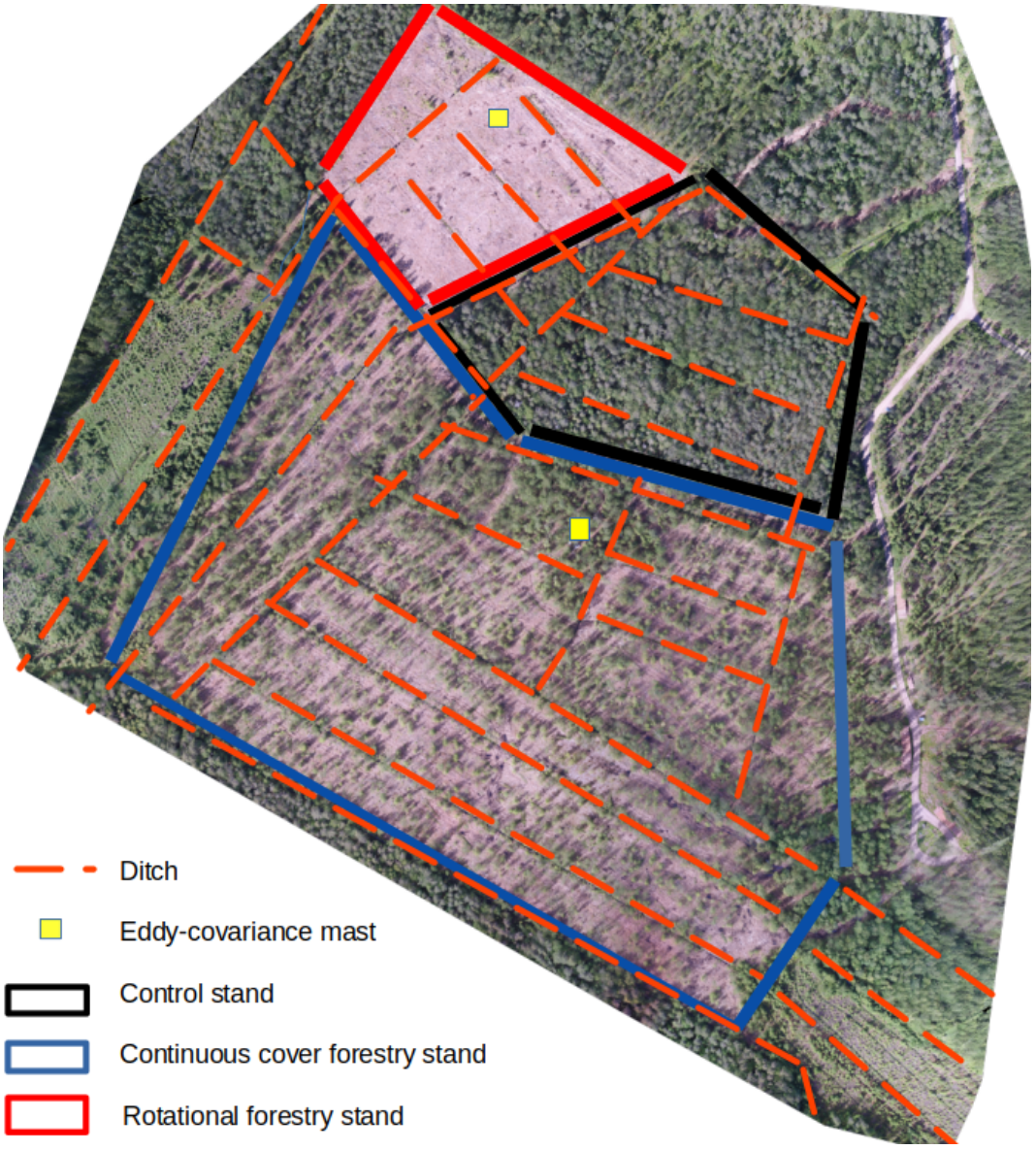

Figure A1. Aerial view of the Lettosuo site. Control, continuous cover forestry and rotational forestry stand are shown in black, blue and red boxes. Yellow squares mark the locations of the Eddy-covariance mast and orange dashed lines are showing the ditch network.

https://doi.org/10.5194/egusphere-2025-5197
Preprint. Discussion started: 30 January 2026

A2 Sensitivity test

Table A1: Sets of parameters used in sensitivity test for soil processes (MeTr^x module).

Variable	Description	range
	Set 1	
BETA LITTER TYPE	Exponential factor for litter decomposition reduction depending on lignin concentration	1 - 3
KR DC HUM1	Decomposition constant of labile humus	2×10^{-3} - 0.03
KR DC HUM2	Decomposition constant of recalcitrant young humus	5×10^{-5} - 3×10^{-3}
KR DC HUM3	Decomposition constant of recalcitrant old humus	1×10^{-6} - 1.25×10^{-4}
KR DC LIG	Decomposition constant of lignin	5×10^{-3} - 0.05
KR DC RAW LITTER	Decomposition constant of raw litter	5×10^{-3} - 0.1
KR DC CEL	Decomposition constant of cellulose	0.05 - 1
KR DC SOL	Decomposition constant of solutes	0.1 - 0.8
KR DC WOOD	Decomposition constant of wood	5×10^{-5} - 1×10^{-3}
	Set 2	
KR REDUCTION ANVF	Decomposition reduction due anaerobicity	0.01 - 1.2
CO2 PROD DECOMP	Instantaneous production of CO2 during decomposition	0.1 - 0.6
KR REDUCTION CN	Decomposition reduction due to C:N ratio	1×10^{-3} - 0.01
F DECOMP T EXP1	Factor for temperature dependency of decomposition	0.5 - 5
F DECOMP T EXP2	Factor for temperature dependency of decomposition	25 - 45
F DECOMP PH1	Factor for pH dependency of decomposition	0.5 - 5
F DECOMP PH2	Factor for pH dependency of decomposition	0.1 - 5
F DECOMP M WEIBULL1	Factor for water filled pore space dependency of decomposition	0 - 0.9
F DECOMP M WEIBULL2	Factor for water filled pore space dependency of decomposition	5 - 15
	Set 3	
KR HU AORG HUM1	Rate constant for humification of active organic material to labile humus	5×10^{-4} - 0.1
KR HU AORG HUM2	Rate constant for humification of active organic material to recalcitrant young humus	1×10^{-5} - 0.01
KR HU CEL	Rate constant for humification of cellulose to labile humus	1×10^{-4} - 0.01
KR HU SOL	Rate constant for humification of solutes to labile humus	1×10^{-4} - 0.01

https://doi.org/10.5194/egusphere-2025-5197
Preprint. Discussion started: 30 January 2026

Variable	Description	range
KR HU DOC	Rate constant for humification of dissolved carbon to labile humus	0 - 0.3
KR HU HUM1	Rate constant for humification of labile humus to recalcitrant young humus	5×10^{-4} - 0.1
KR HU HUM2	Rate constant for humification of recalcitrant young humus to recalcitrant old humus	1×10^{-5} - 0.01
KR HU LIG	Rate constant for humification of lignin	1×10^{-3} - 0.1
METRX CN FRAC HUM3	C:N ratio fraction of humus 3 pool in relation to soil C:N ratio	0 - 1

https://doi.org/10.5194/egusphere-2025-5197
Preprint. Discussion started: 30 January 2026

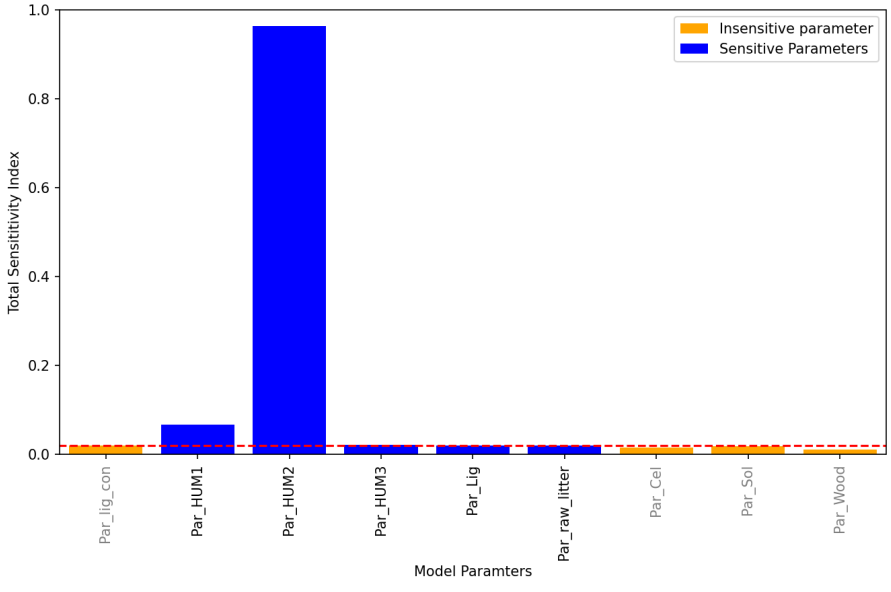

Figure A2. Sensitivity tests for the first set of parameters. Black x-ticks represents the five most sensitive parameters indicated by FAST algorithm and red dashed line indicate the threshold point in the Total sensitivity index for the fifth sensitive parameter. Threshold point for sensitive parameter is dependent on the user definition of number of sensitive parameter (e.g. in this case 5, but could have been any number between 1-9) in the algorithm. Grey x-ticks shows the non-sensitive parameters indicated by FAST.

https://doi.org/10.5194/egusphere-2025-5197
Preprint. Discussion started: 30 January 2026

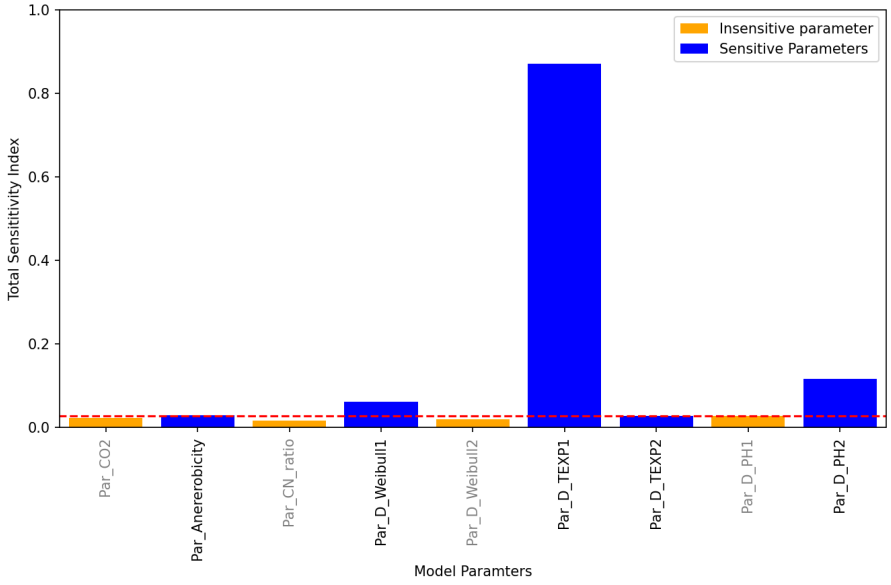

Figure A3. Sensitivity tests for the second set of parameters. Black x-ticks represents the five most sensitive parameters indicated by FAST algorithm and red dashed line indicate the threshold point in the Total sensitivity index for the fifth sensitive parameter. Grey x-ticks shows the non-sensitive parameters indicated by FAST.

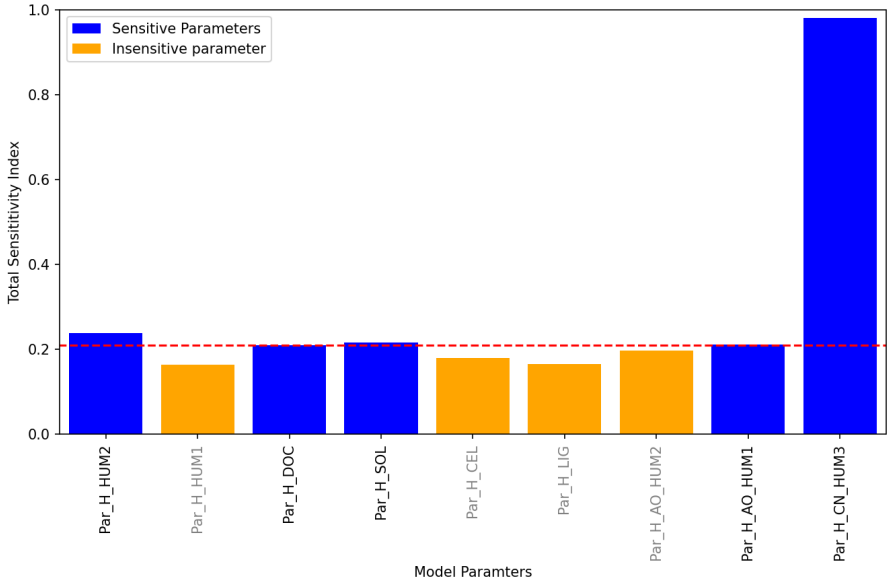

Figure A4. Sensitivity tests for the 3rd set of parameters. Black x-ticks represents the five most sensitive parameters indicated by FAST algorithm and red dashed line indicate the threshold point in the Total sensitivity index for the fifth sensitive parameter. Grey x-ticks shows the non-sensitive parameters indicated by FAST.

https://doi.org/10.5194/egusphere-2025-5197
Preprint. Discussion started: 30 January 2026

A3 Parameters for simulations

Table A2: Selected parameters for species and soil processes and values used in running simulations.

Variable	Description	Adapted Value
	Forest floor	
DLEAFSHED	Total leaf longevity from the first day of emergence	300
GDDFOLSTART	Minimum temperature sum for foliage activity onset (°C)	0
KM20	Maintenance coefficient at reference temperature	1
VCMAX25	Maximum RubP saturated rate of carboxylation at 25°C for sun leaves $\mu mol\ m^{-2}\ s^{-1}$	66.8
SLAMAX	Specific leaf area in the shade ($m^2\ kg^{-1}$)	17 (*)
SLAMIN	Specific leaf area under full light ($m^2\ kg^{-1}$)	7 (*)
	Pine *(Pinus Sylvestris)*	
KM20	Maintenance coefficient at reference temperature	0.455
VCMAX25	Maximum RubP saturated rate of carboxylation at 25°C for sun leaves $\mu mol\ m^{-2}\ s^{-1}$	110.8
SLAMAX	Specific leaf area in the shade ($m^2\ kg^{-1}$)	15.1
SLAMIN	Specific leaf area under full light ($m^2\ kg^{-1}$)	3.4
	Spruce *(Picea Abies)*	
KM20	Maintenance coefficient at reference temperature	0.75
VCMAX25	Maximum RubP saturated rate of carboxylation at 25°C for sun leaves $\mu mol\ m^{-2}\ s^{-1}$	60.9
SLAMAX	Specific leaf area in the shade ($m^2\ kg^{-1}$)	8.3
SLAMIN	Specific leaf area under full light ($m^2\ kg^{-1}$)	3.8
	Birch *(Betula pendula/Pubescens)*	
DLEAFSHED	Total leaf longevity from the first day of emergence	300
GDDFOLSTART	Minimum temperature sum for foliage activity onset (°C)	111
KM20	Maintenance coefficient at reference temperature	0.07
VCMAX25	Maximum RubP saturated rate of carboxylation at 25°C for sun leaves $\mu mol\ m^{-2}\ s^{-1}$	38.4
SLAMAX	Specific leaf area in the shade ($m^2\ kg^{-1}$)	13
SLAMIN	Specific leaf area under full light ($m^2\ kg^{-1}$)	6.2

https://doi.org/10.5194/egusphere-2025-5197
Preprint. Discussion started: 30 January 2026

Variable	Description	Adapted value
	Soil parameters	
CO2 PROD DECOMP	Instantaneous production of CO_2 during decomposition	0.35
F DECOMP T EXP 1	Factor for temperature dependency of decomposition	4
KR DC HUM 1	Decomposition constant of labile humus	0.03
KR DC HUM 2	Decomposition constant of recalcitrant young humus	3×10^{-3}
KR DC HUM 3	Decomposition constant of recalcitrant old humus	1.25×10^{-4}
KR DC RAW LITTER	Decomposition constant of raw litter	0.01
KR DC WOOD	Decomposition constant of wood	1×10^{-3}
KR FRAG ABOVE	Fragmentation constant of above-ground litter	0.01
KR FRAG BELOW	Fragmentation constant of below-ground litter	0.01
METRX MUEMAX C CH4 OX	Growth rate of methane oxidation microbes	0.60
METRX MUEMAX C CH4 PROD	Growth rate of methanogenic microbes	0.38
Ψ	Groundwater lateral gradient	28.7 (38.7)

* 17 for pristine.

https://doi.org/10.5194/egusphere-2025-5197
Preprint. Discussion started: 30 January 2026

Code and data availability. Simulation, measurement data and python codes are available at https://doi.org/10.5281/zenodo.17397308 (Shahriyer et al., 2025a). SPOTPY library can be found from the online python repository at https://doi.org/10.1371/journal.pone.0145180 (Houska et al., 2015). Simulation setup can be found at https://doi.org/10.5281/zenodo.17987219 (Shahriyer et al., 2025b). Model source code can be found at https://www.radar-service.eu/radar/en/dataset/8w3v0bf96c2xzenj?token=gekSBjqBudDNCrBOiiSX (Shahriyer et al., 2025c).

Author contributions. Model setup and running the simulations, data analysis, and writing of the article was done by AS with the support of TA, TM and DK. TA, TM, and AL conceptualized the study. Modifications to the model source code was done by DK and RG. MK and HR provided the measurement data, maintained the measurement systems and contributed to the text. Initial model setup, data analysis and reviewing of the text was done by SO, YG and HK. All coauthors contributed to the final reviews of the text.

Competing interests. The contact author has declared that none of the authors has any competing interests.

Acknowledgements. We are grateful for all the support that has enabled us to carry out the research. This project has received funding from the MMM Grant no. 4400T-2105 (TURNEE), and JTF-EP TUPSU. we are grateful for the support of the ACCC Flagship funded by the Research Council of Finland (grant no. 337552) and the Ministry of Transport and Communications through the Integrated Carbon Observation System (ICOS) and ICOS Finland (FIRI - ICOS Finland (345531)). This project further received funding from the European Union – NextGenerationEU instrument and was funded by the Research Council of Finland under grant no. 347794 (ForClimate), 324259 (BiBiFe), 341752 (RESPEAT). Horizon Europe Framework Program of the European Union with grant no. 101056844 (Alfawetlands) and 101056848 (Wethorizons). Minor modification to the text was done with the help of perplexity.ai.

https://doi.org/10.5194/egusphere-2025-5197
Preprint. Discussion started: 30 January 2026

References

Aalto, J., Pirinen, P., , and Jylhä, K.: New gridded daily climatology of Finland: Permutation-based uncertainty estimates and temporal trends in climate, J. Geophys. Res. Atmos, 121, 3807–3823, https://doi.org/10.1002/2015JD024651, 2016.

Cade, S. M., Clemitshaw, K. C., Molina-Herrera, S., Grote, R., Haas, E., Wilkinson, M., Morison, J. I. L., and Yamulki, S.: Evaluation of LandscapeDNDC Model Predictions of CO_2 and N_2O Fluxes from an Oak Forest in SE England, Forests, 12,1517, https://doi.org/10.3390/f12111517, 2021.

Clarke, D. and Rieley, J.: Strategy for Responsible Peatland Management, International Peat Society, 2019.

Dirnböck, T., Kobler, J., Kraus, D., Grote, R., and Kiese, R.: Impacts of management and climate change on nitrate leaching in a forested karst area, Journal of Environmental Management, 165, 243–252, https://doi.org/10.1016/j.jenvman.2015.09.039, 2016.

Dirnböck, T., Kraus, D., Grote, R., Klatt, S., J.Kobler, Schindlbacher, A., Seidl, R., Thom, D., and Kies, R.: Substantial understory contribution to the C sink of a European temperate mountain forest landscape, Landscape Ecol, 35, 483–499, https://doi.org/10.1007/s10980-019-00960-2, 2020.

Findlay, S. E.: Chapter 4 - Organic Matter Decomposition, in: Fundamentals of Ecosystem Science (Second Edition), edited by Weathers, K. C., Strayer, D. L., and Likens, G. E., pp. 81–102, Academic Press, second edition edn., ISBN 978-0-12-812762-9, https://doi.org/https://doi.org/10.1016/B978-0-12-812762-9.00004-6, 2021.

Grote, R., Mayrhofer, S., Fischbach, R., Steinbrecher, R., Staudt, M., and Schnitzler, J.-P.: Process-based modelling of isoprenoid emissions from evergreen leaves of Quercus ilex (L.), Atmospheric Environment, 40, S152–S165, https://doi.org/10.1016/j.atmosenv.2005.10.07, 2006.

Grote, R., Lavoir, A.-V., Rambal, S., Staudt, M., Zimmer, I., and Schnitzler, J.-P.: Modelling the drought impact on monoterpene fluxes from an evergreen Mediterranean forest canopy, Oecologia, 160, 213–223, https://doi.org/10.1007/s00442-009-1298-9, 2009.

Grote, R., Kiese, R., Grünwald, T., Ourcival, J.-M., and Granier, A.: Modelling forest carbon balances considering tree mortality and removal, Agricultural and Forest Meteorology, 151, 179–190, https://doi.org/10.1016/j.agrformet.2010.10.002, 2011.

Haas, E., Klatt, S., Fröhlich, A., Kraft, P., Werner, C., Kiese, R., Grote, R., Breuer, L., and Butterbach-Bahl, K.: LandscapeDNDC: a process model for simulation of biosphere–atmosphere–hydrosphere exchange processes at site and regional scale, Landscape Ecol, 28, 615–636, https://doi.org/10.1007/s10980-012-9772-x, 2013.

Haas, E., Carozzi, M., Massad, R. S., Butterbach-Bahl, K., and Scheer, C.: Long term impact of residue management on soil organic carbon stocks and nitrous oxide emissions from European croplands, Science of the Total Environment, 836 (2022) 154932, https://doi.org/10.1016/j.scitotenv.2022.154932, 2022.

Harmens, H., Norris, D., Cooper, D., Mills, G., Steinnes, E., Kubin, E., Thöni, L., Aboal, J., Alber, R., Carballeira, A., Coşkun, M., Temmerman, L. D., Frolova, M., González-Miqueo, L., Jeran, Z., Leblond, S., Liiv, S., Mankovská, B., Pesch, R., Poikolainen, J., Rühling, Å., Santamaria, J., Simonèiè, P., Schröder, W., Suchara, I., Yurukova, L., and Zechmeister, H.: Nitrogen concentrations in mosses indicate the spatial distribution of atmospheric nitrogen deposition in Europe, Environmental Pollution, 159, 2852–2860, https://doi.org/10.1016/j.envpol.2011.04.041, 2011.

Houska, T., Kraft, P., Chamorro-Chavez, A., and Breuer, L.: SPOTting Model Parameters Using a Ready-Made Python Package, https://doi.org/10.1371/journal.pone.0145180, 2015.

Houska, T., Kraus, D., Kiese, R., and Breuer, L.: Constraining a complex biogeochemical model for multi-site greenhouse gas emission simulations by model-data fusion, Biogeosciences Discuss., https://doi.org/10.5194/bg-2017-96, 2017, 2017.

https://doi.org/10.5194/egusphere-2025-5197
Preprint. Discussion started: 30 January 2026

Huttunen, J. T., Nykänen, H., Martikainen, P. J., and Nieminen, M.: Fluxes of nitrous oxide and methane from drained peatlands following forest clear-felling in southern Finland, Plant and Soil, 255, 457–462, 2003.

Hytönen, J., Hökkä, H., and Saarinen, M.: The effect of planting, seeding and soil preparation on the regeneration success of Scots pine (Pinus sylvestris L.) on drained peatlands – 10-year results, Forestry Studies | Metsanduslikud Uurimused, 72, 91–106, https://doi.org/10.2478/fsmu-2020-0008, 2020.

Korkiakoski, M., Tuovinen, J.-P., Aurela, M., Koskinen, M., Minkkinen, K., Ojanen, P., Penttilä, T., Rainne, J., Laurila, T., and Lohila, A.: Methane exchange at the peatland forest floor – automatic chamber system exposes the dynamics of small fluxes, Biogeosciences, 14, 1947–1967, 2017, 14, 1947–1967, 2017.

Korkiakoski, M., Tuovinen, J.-P., Penttilä, T., Sarkkola, S., Ojanen, P., Minkkinen, K., Rainne, J., Laurila, T., , and Lohila, A.: Greenhouse gas and energy fluxes in a boreal peatland forest after clear-cutting, Biogeosciences, 16, 3703–3723, 2019.

Korkiakoski, M., Ojanen, P., Penttilä, T., Minkkinen, K., Sarkkola, S., Rainne, J., Laurila, T., and Lohila, A.: Impact of partial harvest on CH4 and N2O balances of a drained boreal peatland forest, Agricultural and Forest Meteorology, 295 (2020) 108168, 2020.

Korkiakoski, M., Ojanen, P., Tuovinen, J.-P., Minkkinen, K., Nevalainen, O., Penttilä, T., Aurela, M., Laurila, T., and Lohila, A.: Partial cutting of a boreal nutrient-rich peatland forest causes radically less on-site CO2 emissions than clear-cutting, Agricultural and Forest Meteorology, 332 (2023) 109361, 2023.

Kraus, D., Weller, S., Klatt, S., Haas, E., Wassmann, R., Kiese, R., and Butterbach-Bahl, K.: A new LandscapeDNDC biogeochemical module to predict CH_4 and N_2O emissions from lowland rice and upland cropping systems, Plant Soil, 386, 125–149, https://doi.org/10.1007/s11104-014-2255-x, 2015.

Laiho, R.: Decomposition in peatlands: Reconciling seemingly contrasting results on the impacts of lowered water levels., Soil Biology and Biochemistry, 38(8), 2011–2024, 2006.

Laine, J.: Metsäojitettujen soiden luokittelu (Classification of forest drained peatlands), Suo, 40(1), 37–51, http://suo.fi/article/9651, 1989.

Laurén, A., Palviainen, M., Launiainen, S., Leppä, K., Stenberg, L., Urzainki, I., Nieminen, M., Laiho, R., and Hökkä, H.: Drainage and Stand Growth Response in Peatland Forests—Description, Testing, and Application of Mechanistic Peatland Simulator SUSI, Forests, 12,293, https://doi.org/10.3390/f12030293, 2021.

Lehtonen, I. and Pirinen, P.: 2018: An exceptionally dry thermal growing season in Finlands, FMI's Climate Bulletin: Research Letters, 1(1), 6, https://doi.org/10.35614/ISSN-2341-6408-IK-2019-04-RL, 2019.

Leppä, K., Korkiakoski, M., Nieminen, M., Laiho, R., Hotanen, J.-P., Kieloaho, A.-J., Korpela, L., Laurila, T., Lohila, A., Minkkinen, K., Mäkipää, R., Ojanen, P., Pearson, M., Penttilä, T., Tuovinen, J.-P., and Launiainen, S.: Vegetation controls of water and energy balance of a drained peatland forest: Responses to alternative harvesting practices, Agricultural and Forest Meteorology, 295 (2020) 108198, 2020.

Li, X., Markkanen, T., Korkiakoski, M., Lohila, A., Leppänen, A., Aalto, T., Peltoniemi, M., Mäkipää, R., Kleinen, T., and Raivonen, M.: Modelling alternative harvest effects on soil CO2 and CH4 fluxes from peatland forests, Science of Total Environment, 951, https://doi.org/10.1016/tj.scititenv.2024.175257, 2024.

Liu, C., Wang, Q., Mäkelä, A., Hökkä, H., Peltoniemi, M., and Hölttä, T.: A model bridging waterlogging, stomatal behavior and water use in trees in drained peatland, Tree physiology, 42, 1736–1749, https://doi.org/10.1093/treephys/tpac037, 2022.

Lohila, A., Minkkinen, K., Aurela, M., Tuovinen, J.-P., Penttilä, T., Ojanen, P., and Laurila, T.: Greenhouse gas flux measurements in a forestry-drained peatland indicate a large carbon sink, Biogeosciences, 8, 3203–3218, https://doi.org/10.5194/bg-8-3203-2011, 2011.

Makrickas, E., Manton, M., Angelstam, P., and Grygoruk, M.: Trading wood for water and carbon in peatland forests? Rewetting is worth more than wood production, Journal of Environmental Management, 341, 117 952, https://doi.org/10.1016/j.jenvman.2023.117952, 2023.

https://doi.org/10.5194/egusphere-2025-5197
Preprint. Discussion started: 30 January 2026

Mezbahuddin, M., Grant, R. F., and Flanagan, L. B.: Coupled eco-hydrology and biogeochemistry algorithms enable the simulation of water table depth effects on boreal peatland net CO2 exchange, Biogeosciences, 14, 5507–5531, https://doi.org/10.5194/bg-14-5507-2017, 2017.

Minkkinen, K. and Laine, J.: Vegetation heterogeneity and ditches create spatial variability in methane fluxes from peatlands drained for forestr, Plant Soil, 285, 289–304, https://doi.org/10.1007/s11104-006-9016-4, 2006.

Molina-Herrera, S., Grote, R., Santabárbara-Ruiz, I., Kraus, D., Klatt, S., Haas, E., Kiese, R., and Butterbach-Bahl, K.: Simulation of CO2 Fluxes in European Forest Ecosystems with the Coupled Soil-Vegetation Process Model "LandscapeDNDC", Forests, 6, 1779–1809, https://doi.org/10.3390/f6061779, 2015.

Mozafari, B., Bruen, M., Donohue, S., Renou-Wilson, F., and O'Loughlin, F.: Peatland dynamics: A review of process-based models and approaches, Science of the Total Environment, 877, https://doi.org/10.1016/j.scitotenv.2023.162890, 2023.

Nevalainen, O.: ollinevalainen/satellitetools: v1.0.0, a, https://doi.org/10.5281/ZENODO.5993292, 2022.

Nichols, J. E. and Peteet, D. M.: Rapid expansion of northern peatlands and doubled estimate of carbon storage, Nature Geoscience, 12, 917–921, https://doi.org/10.1038/s41561-019-0454-z, 2019.

Nieminen, M., Hökkä, H., Laiho, R., Juutinen, A., Ahtikoski, A., Pearson, M., Kojola, S., Sarkkola, S., Launiainen, S., Valkonen, S., Penttilä, T., Lohila, A., Saarinen, M., Haahti, K., Mäkipää, R., Miettinen, J., and Ollikainen, M.: Could continuous cover forestry be an economically and environmentally feasible management option on drained boreal peatlands?, Forest Ecology and Management, 424, 78–84, https://doi.org/10.1016/j.foreco.2018.04.046, 2018.

Ojanen, P., Minkkinen, K., and Penttilä, T.: The current greenhouse gas impact of forestry-drained boreal peatlands, Forest Ecology and Management, 289, 201–208, https://doi.org/10.1016/j.foreco.2012.10.008, 2013.

Sarkkola, S., Hökkä, H., Koivusalo, H., Nieminen, M., Ahti, E., Päivänen, J., and Laine, J.: Role of tree stand evapotranspiration in maintaining satisfactory drainage conditions in drained peatlands, Canadian Journal of Forest Research, 40, https://doi.org/10.1139/X10-084, 2010.

Shahriyer, A. H., Kraus, D., Markkanen, T., Korkiakoski, M., Rautakoski, H., Orttenvuori, S., Gao, Y., Kajasilta, H., Grote, R., Lohila, A., and Aalto, T.: Dataset and python codes: Evaluation of the LandscapeDNDC model for drained peatland forest managements, LDNDC v1.35.2 (revision 11434), https://doi.org/10.5281/zenodo.17397308, 2025a.

Shahriyer, A. H., Kraus, D., Markkanen, T., Korkiakoski, M., Rautakoski, H., Orttenvuori, S., Gao, Y., Kajasilta, H., Grote, R., Lohila, A., and Aalto, T.: Simulation setup: Evaluation of the LandscapeDNDC model for drained peatland forest managements, LDNDC v1.35.2 (revision 11434), https://doi.org/10.5281/zenodo.17987219, 2025b.

Shahriyer, A. H., Kraus, D., Markkanen, T., Korkiakoski, M., Rautakoski, H., Orttenvuori, S., Gao, Y., Kajasilta, H., Grote, R., Lohila, A., and Aalto, T.: Simulation model code: Evaluation of the LandscapeDNDC model for drained peatland forest managements, LDNDC v1.35.2 (revision 11434), 2025c.

Shi, X., Ricciuto, D. M., Thornton, P. E., Xu, X., Yuan, F., Norby, R. J., Walker, A. P., Warren, J. M., Mao, J., Hanson, P. J., Meng, L., Weston, D., and Griffiths, N. A.: Extending a land-surface model with Sphagnum moss to simulate responses of a northern temperate bog to whole ecosystem warming and elevated CO2, Biogeosciences, 18, 467–486, https://doi.org/10.5194/bg-18-467-2021, 2021.

Silva, M. P., Healy, M. G., and Gill, L.: Reviews and syntheses: A scoping review evaluating the potential application of ecohydrological models for northern peatland restoration, Biogeosciences, 21, 3143–3163, https://doi.org/10.5194/bg-21-3143-2024, 2024.

Simola, H., Pitkänen, A., and Turunen, J.: Carbon loss in drained forestry peatlands in Finland, estimated by re-sampling peatlands surveyed in the 1980s, European Journal of Soil Science, https://doi.org/10.1111/j.1365-2389.2012.01499.x, 2012.

https://doi.org/10.5194/egusphere-2025-5197
Preprint. Discussion started: 30 January 2026

Turunen, J. and Valpola, S.: The influence of anthropogenic land use on Finnish peatland area and carbon stores 1950–2015, Mires and Peat, 26, https://doi.org/10.19189/MaP.2019.GDC.StA.1870, 2020.

Vasander, H. and Laine, J.: Site type classification on drained peatlands, Korhonen, R., Korpela, L., Sarkkola, S. (Eds.). Finland – Fenland: Research and Sustainable Utilisation of Mires and Peat. Finnish Peatland Society, Maahenki Ltd., Helsinki, pp. 146–151, 2008.

Werner, C., Haas, E., Grote, R., Gauder, M., Graeff-Hönninger, S., Claupein, W., and Butterbach-Bahl, K.: Biomass production potential from Populus short rotation systems in Romania, GCB Bioenergy, 4, no 6, 642–653, https://doi.org/10.1111/j.1757-1707.2012.01180.x, 2012.